nature reviews materials

https://doi.org/10.1038/s41578-024-00715-9

Review article

Check for updates

Diffusion mechanisms of fast lithium-ion conductors

KyuJung Jun [1,2], Yu Chen [1,2], Grace Wei [1,2], Xiaochen Yang [1,2] & Gerbrand Ceder [1,2]

Abstract

The quest for next-generation energy-storage technologies has pivoted towards all-solid-state batteries, primarily owing to their potential for enhanced safety and energy density. At the centre of this promising technology lie inorganic lithium superionic conductors, which facilitate rapid ion transport comparable to that in their liquid counterparts. Despite their promise, the limited availability of materials that both achieve superionic conductivity and fulfil all practical requirements necessitates the discovery of novel conductors. This Review comprehensively explores the diverse structural and chemical factors that improve ionic conductivity and the atomistic mechanism by which each factor affects it. We emphasize the importance of a dual approach: using structural factors to enable high-conducting prototypes, and chemical factors to further optimize the ionic conductivity. From these insights, we distil over 40 years of conductor development history to the key concepts that paved the way for today's leading superionic conductors. In detailing the trajectory of ionic conduction advancements, this Review not only charts the progress in the field but also proposes a strategic approach for researchers to efficiently innovate with the ultimate goal of realizing the promise of all-solid-state batteries.

Sections

[1]Department of Materials Science and Engineering, University of California, Berkeley, CA, USA. [2]Materials Sciences Division, Lawrence Berkeley National Laboratory, Berkeley, CA, USA. e-mail: gceder@berkeley.edu

Introduction

Solid-state materials exhibiting fast lithium-ion transport are pivotal in enabling the next generation of energy-storage devices[1]. The all-solid-state battery is at the centre of a paradigm shift whereby traditional flammable liquid electrolytes are substituted by inorganic solids, promising substantial enhancements in safety[2]. In addition, improvements in energy density are foreseen when solid electrolytes enable lithium metal anodes[3] or anode-free designs[4].

Lithium superionic conductors serve as the foundation for such technological innovations[5]. The term superionic conductor refers to materials with exceptionally high ionic conductivity[6,7], typically surpassing 0.1 mS cm^{-1} at room temperature. A major characteristic of inorganic crystalline ionic conductors is that the transference number, which reflects the fraction of the current carried by the Li-ion carriers, reaches unity[8] because the anion groups and non-lithium cations are typically immobile. A transference number of unity has a positive influence on the power characteristics of an electrochemical cell, as no concentration polarization is possible in the conductor[8]. This is in contrast to liquid electrolytes in which a lithium salt such as $LiPF_6$ dissociates in an organic solvent, resulting in both positive and negative ions being mobile. Similarly, in polymer electrolytes such as LiTFSI dissolved in PEO, Li-ion diffusion occurs via the solvation of lithium ions by polymer chains[9]. The diffusion mechanisms in liquid and polymer electrolytes differ considerably from the ones in inorganic crystalline materials, and we refer to other review articles on such topics[9,10]. In this Review, we exclusively discuss the Li-ion diffusion mechanisms in inorganic crystalline structures.

Although this Review focuses on the lithium ionic conductivity of inorganic solids, various other properties must practically be considered when used in an electrochemical cell. For example, a solid electrolyte separator in an all-solid-state battery also requires low electronic conductivity and good stability against contacting components (cathode active particles, carbon and anode). Recently, a trend has emerged to use different solid conductors as separator and additive in the cathode[11–13]. This may reduce demands on the separator material in terms of chemical and mechanical stability against the cathode chemistry and its high oxidation potential. Catholyte materials that do not come in contact with the anode would then only require good anodic stability and chemical stability with cathode active materials, as well as facilitating deformation induced by the volume changes arising from the cathode cycling[11,14]. Although solid electrolyte development focuses mostly on their integration with Li-ion batteries, additional requirements can emerge when they are used in new technologies such as solid-state Li–air batteries, where stability against Li peroxide or hydroxide, alkaline environments and humidity may be necessary[15,16].

Besides the property requirements for solid electrolytes, economic and manufacturing factors such as precursor price, elemental scarcity, cell processability, stability and safety are important considerations during the final stage of the design process, potentially ruling out many of the currently known materials with high ionic conductivity. As of now, among known superionic conductors, no single material fulfils all the required attributes, which can lead to significant engineering and processing challenges. Examples of this are the need to protect sulfide-based conductors from moisture during processing to prevent release of H_2S, or the high temperatures required to sinter some oxide-based conductors. For these reasons, it is critical to enlarge the choice of possible solid-state electrolytes through the development of systematic and rational design principles for fast Li-ion diffusion.

Lithium-ion diffusion in crystalline inorganic structures occurs via discrete or small-group hopping events that occur stochastically from thermal vibrational motion. Sites for lithium ions are typically well defined by the geometry of the immobile crystal structure. The ionic conductivity is typically expressed as $\sigma = \frac{\sigma_0}{T}\exp(-\frac{E_a}{kT})$ where σ_0 corresponds to the pre-exponential factor and E_a is the activation energy[17]. In the dilute carrier regime, σ_0 scales with the number of free carriers and E_a consists mostly of the carrier's migration energy (potentially augmented with binding energies arising from a dopant used to introduce the carrier), but most superionic lithium conductors are far from this regime and have a high concentration of lithium ions in the solid participating in the transport process. This can make σ_0 and E_a more difficult to interpret and can even lead to changes in activation energy with temperature[18–20]. When designing superionic conductors, one aims to directly maximize the room-temperature ionic conductivity or minimize the activation energy, as a low activation energy below 0.4 eV is typically required to achieve a room-temperature ionic conductivity of at least 0.1 mS cm^{-1} (refs. 21,22).

Various experimental techniques can probe ion transport in a crystal lattice at a wide range of length scales and timescales[23]. Electrochemical impedance spectroscopy (EIS) is the most common and direct method to measure ionic conductivity on the macroscopic scale. With equivalent circuit fitting analysis, such EIS measurements can be used to distinguish ion conduction processes within the grain and across grain boundaries[24] or distinguish contributions from ions and electrons[25]. Tracer diffusion can be measured by using isotope detection techniques such as time-of-flight secondary ion mass spectroscopy, mass spectrometry, magnetic resonance imaging and neutron depth profiling, resulting in element-specific tracer diffusion coefficients[23]. Pulsed field-gradient nuclear magnetic resonance (PFG-NMR) is also element specific and can be used to probe self-diffusion coefficients[26]. For microscopic ion transport, solid-state NMR is a versatile tool to study local ion jump frequencies and random-walk diffusion coefficients by line shape analysis at variable temperatures and NMR relaxometry[27]. Quasi-elastic neutron scattering[28] and muon spin relaxation[29] can be used to probe ion diffusion on the atomic scale. In addition, nonlinear optical methods have recently been reported to directly probe ion hops on the picosecond timescale[30,31]. These local ion hopping dynamics cannot be directly probed by EIS, which can be influenced by factors such as grain boundaries and porosities.

Computational techniques are widely used to shed light on the atomistic diffusion mechanisms in fast Li-ion conductors. Molecular dynamics simulations where a structure is simulated in a given thermodynamic ensemble provide estimates of the Li-ion diffusion coefficient and insights into the atomistic diffusion mechanism[32]. Nudged elastic band calculations[33,34] also serve an important role in revealing the pathway-dependent Li-ion migration barrier to estimate the macroscopic activation energy of diffusion. Other empirical heuristics such as bond valence sums[35,36] or electrostatic Ewald energies[37] provide valuable insights for understanding ion diffusion channels but fail to provide quantitative estimations of ionic conductivities.

Diffusion in molecular dynamics simulations can be analysed by Onsager coefficients L_{ij} in the Onsager transport equation[38–40]. As non-lithium cations and anions are typically immobile in inorganic crystalline superionic conductors, we can ignore all the correlation terms between them and lithium ions. Thus, the ionic conductivity can be computed exactly as $\sigma = F^2z^2(L_{Li^+}^{self} + L_{Li^+}^{distinct})$ where F and z correspond to Faraday's constant and the charge of the mobile ion species. Conventionally, $L_{Li^+}^{distinct}$, which is related to the motion of the centre of mass

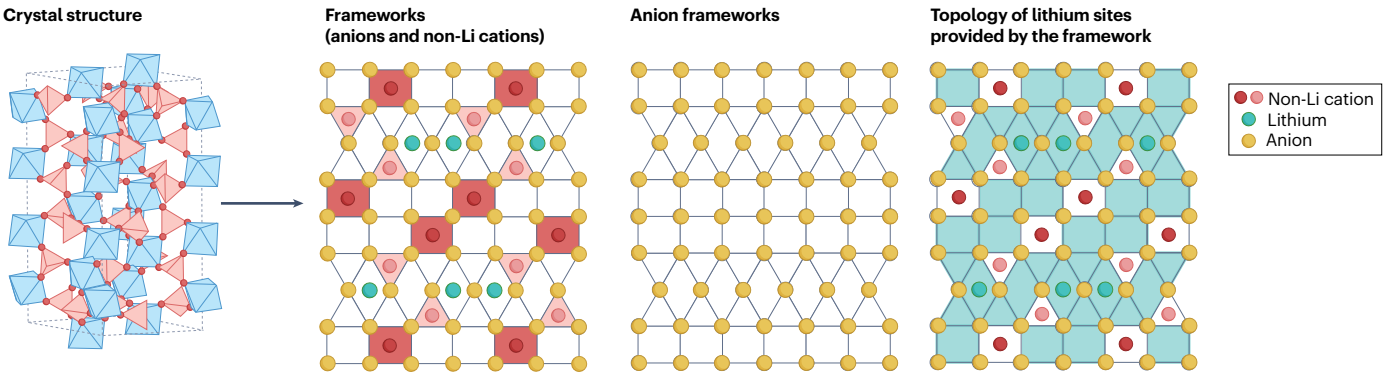

Fig. 1 | Static structural factors that govern Li-ion diffusion in inorganic crystalline materials. Each triangle, rectangle or trapezoid is a 2D illustration of possible cation interstitial sites provided by the anion framework (yellow circles). The green circles and polygons represent Li ions and the sites that they can potentially occupy. The red and pink circles and polygons represent non-Li cations and the sites that are occupied by them. Adapted from ref. 51, Springer Nature Limited.

of lithium ions, is challenging to converge within the ab initio molecular dynamics simulation timescale. Instead, the Nernst–Einstein relation assuming no correlation between distinct lithium ions ($L_{Li^+}^{distinct} = 0$) is often taken, and only $L_{Li^+}^{self}$ (corresponding to the self-diffusion coefficient) is considered. Nevertheless, deviation of the Nernst–Einstein conductivity from the ionic conductivity (measured by Haven ratio[41]) is not significant, and self-diffusion coefficients serve well in understanding Li-ion transport from molecular dynamics simulations. We refer the readers to another perspective discussing a more complete diffusion theory[42].

The traditional trial-and-error approach[43] has unveiled considerable challenges in the discovery and development of new inorganic superionic conductors. This mainly originates from a lack of design principles that may guide researchers to rationally explore the structural prototypes, compositions, and dopants that can potentially improve the ionic conductivity of a given inorganic material. What makes the trial-and-error approach even more challenging is that each attempt requires navigating unknown synthesis recipes and optimizing processing conditions before the measurement of a material's ionic conductivity. For example, although the lithium garnet prototype was first discovered in 1969 (ref. 44), it was not until 2003 (ref. 45) that it was considered a mediocre Li-ion conductor (0.0034 mS cm^{-1}). Another decade of effort was necessary to achieve the state-of-the-art ionic conductivity of 1 mS cm^{-1} (ref. 46) for the garnet structure. This has led to the pursuit for a more systematic understanding of the factors that govern fast Li-ion diffusion in inorganic crystal structures, in the hope that such design principles can greatly accelerate the discovery of new materials that can serve as solid electrolytes in all-solid-state batteries.

In this Review, we first introduce the structural and topological factors that govern ionic conductivity. The structural factors are divided into two parts: features of the framework and features of individual Li-ion sites. Second, we discuss the chemical factors that are often used to optimize the ionic conductivity in a favourable structural framework. Based on these design principles, we then examine how they have led to the development of various classes of state-of-the-art superionic conductors. Finally, we provide our perspective on how the discovery and optimization of new superionic conductors can be accelerated. This Review intends to combine the individual studies performed on different classes of ionic conductors to provide a global conceptual framework on the various mechanisms that can be used to optimize ionic conductivity in inorganic crystalline materials.

Structural and topological factors

Analysing inorganic crystal structures for Li-ion diffusion

Structural and topological factors typically determine whether a structure can become a superionic conductor, but chemical tuning is often needed to improve the ionic conductivities of compounds that possess desirable structural attributes. This distinction between structural and chemical factors mimics the typical discovery of a conducting class of materials. When a reasonable ionic conductivity is observed in a specific structural prototype, researchers usually begin to apply various chemical modifications, sometimes rewarded with order-of-magnitude improvements in ionic conductivity[47,48]. Compilation of fast-conducting structures has allowed for the extraction of common structural features, allowing researchers to directly search for structures that may allow superionic conductivity[21,49]. In this section, we explain the structural features that have been demonstrated to benefit ionic conductivity.

Typical inorganic crystals can be decomposed into three layers of structural components: an anion framework, the non-Li cation arrangements, and the occupied and potential Li sites (Fig. 1). An anion framework is defined as the sublattice of anions that build the backbone of a crystal structure[50]. The framework anions are generally immobile and determine the geometry of the coordination environment for Li ions and non-Li cations. In most inorganic crystalline superionic conductors, the non-Li cations do not show any long-range mobility. Therefore, we refer to the set of non-Li cation coordination polyhedra as the framework[51]. The non-Li cations rule out part of the interstitial sites provided by the anion framework, leaving a subset of interstitial sites available for Li ions to occupy. In the next subsection, we first examine how frameworks and anion frameworks influence ionic conductivity. Subsequently, we discuss how Li-ion sites determined by the framework affect Li-ion conductivity. Finally, we discuss structures where the framework is rotationally mobile and its implications for Li-ion diffusion.

Anion and cation structural frameworks

If interactions between a migrating lithium ion and the other cations are negligible, then the topology of the anion framework determines

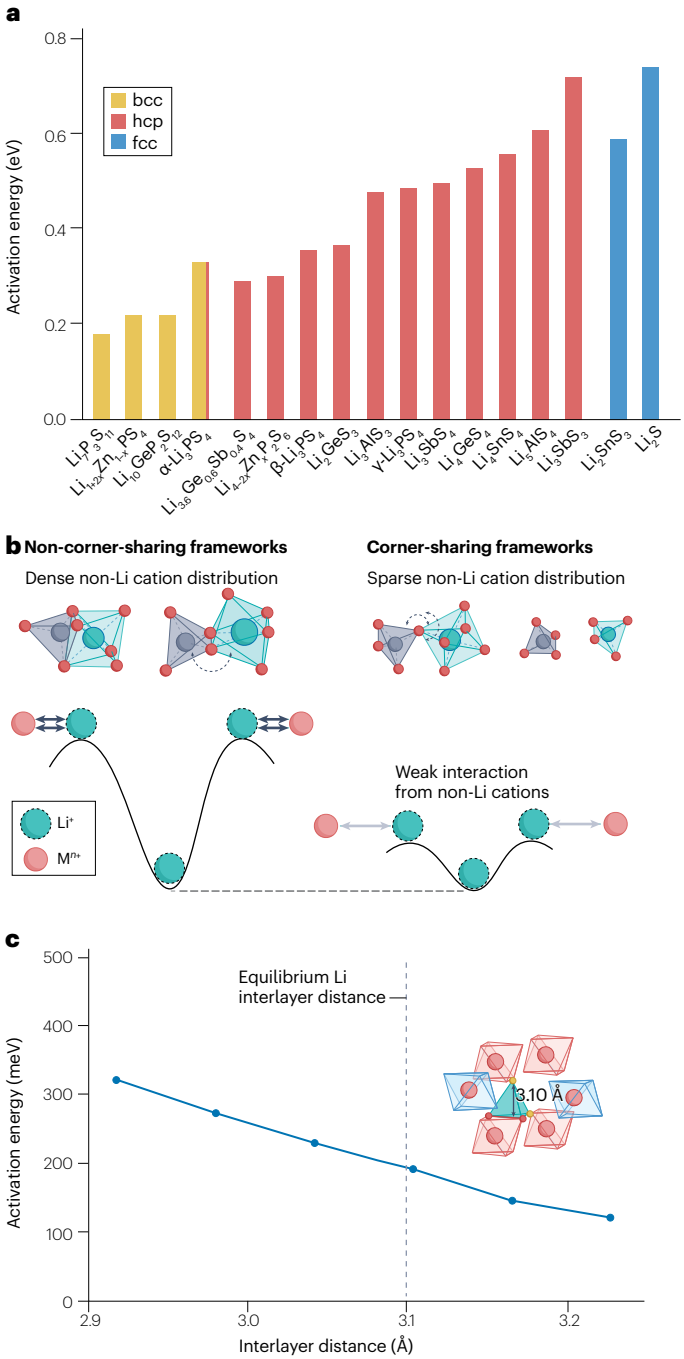

Fig. 2 | Effect of the frameworks on Li-ion diffusion. a, Experimentally measured activation energy for sulfide systems classified by anion framework. α-Li_3PS_4 has 75% body-centred cubic (bcc) and 25% hexagonal close packing (hcp) of sulfur anions. **b**, Comparison of oxides with corner-sharing frameworks and non-corner-sharing frameworks. The sparse spatial distribution of non-Li cations in corner-sharing frameworks reduces the interaction between Li and non-Li cations, resulting in a flattened energy landscape. **c**, Dependence of the activation energy on the interlayer distance in layered hcp chloride superionic conductors. The dashed line shows the equilibrium Li interlayer distance for the disordered model structure shown[86]. fcc, face-centred cubic. Panel **b** adapted from ref. 51, Springer Nature Limited. Panel **c** reprinted with permission from ref. 86, AAAS.

the ionic conductivity. This is important in highly polarizable anion chemistries such as S^{2-}, Se^{2-}, I^- and Br^- where Coulombic interactions between Li ions and other cations are well screened out. Conversely, in weakly screened anion chemistries, the interactions between Li ions and other cations are more prominent, and the ionic conductivity is more affected by the arrangement of the non-Li cations and by Li–Li interactions in the case of highly Li-stuffed conductors. In addition to the effect of polarizability, anion chemistries determine the lattice parameter, which in turn governs inter-cation distance within the lattice. As such, a large anion size often results in a weaker interaction between Li and non-Li cations and therefore a flattened Li-ion diffusion landscape.

Anion framework. The body-centred-cubic (bcc) anion framework is observed prominently in state-of-the-art sulfide ionic conductors such as $Li_{10}GeP_2S_{12}$ (LGPS)[52,53], $Li_7P_3S_{11}$ (refs. 54,55) and α-Li_3PS_4 (refs. 56,57). Computing the migration barrier of a single Li ion in a bcc, face-centred-cubic (fcc) and hexagonal close-packed (hcp) S^{2-} anion framework revealed that[50] for a typical volume regime of 30–50 $Å^3$ per S^{2-}, the bcc anion framework provides the lowest migration barrier, well below 200 meV. The experimentally measured activation energies for fast ionic conducting sulfides with the bcc anion framework correspond well to the migration barriers predicted from this anion framework analysis[50]. In addition, a survey of the experimental activation energy for Li conduction in sulfides[52,55,57–71] shows that a bcc anion framework does indeed provide a lower barrier than close-packed frameworks (Fig. 2a).

The low migration barrier in the bcc anion framework is attributed to the existence of a face-sharing network of distorted tetrahedral sites (tet) within the structure. Using these sites, a Li ion can percolate through the crystal structure with minimal change in its coordination environment, resulting in a flat energy landscape for the Li ion. In fcc and hcp anion frameworks, a Li ion in an octahedral site (oct) must pass through a triangular bottleneck to an intermediate tetrahedral site and then to another triangular bottleneck before reaching an equivalent octahedral site for percolation. The more pronounced change in coordination environments along the Li migration path in fcc and hcp anion frameworks results in higher activation energies. Argyrodites, which are among the fastest inorganic ion conductors, although not bcc-packed, share the same feature of 3D percolating face-sharing tetrahedral sites, which explains their high intrinsic Li mobility[50,72].

Identification of the bcc anion framework as favourable for Li-ion conductivity led to the discovery of numerous sulfide-based superionic conductors. For example, $LiZnPS_4$ was computationally designed to be a superionic conductor based on its bcc-resembling anion framework[73]. On substituting Zn^{2+} with two Li^+, excellent ionic conductivity of up to 0.84 mS cm^{-1} was achieved with the composition $Li_{1+2x}Zn_{1-x}PS_4$ ($x = 0.75$)[58,74].

Although bcc anion frameworks have been computed to have lower migration barriers than hcp and fcc anion frameworks regardless of anion type[50], this does not preclude fast ion transport in fcc or hcp close-packed frameworks. Close-packed (fcc or hcp) crystalline halide materials, notably, show high ionic conductivity at room temperature, σ_{300K}, of more than 1 mS cm^{-1}, with low migration barriers due to their high polarizability and low anion valence compared with oxides and sulfides[75]. Anion framework analysis has shown that the oct–tet–oct pathways in the fcc and hcp (in-plane) anion frameworks have the same activation energy[76]. However, the fcc anion packing in halides has 3D isotropic diffusion channels, whereas the hcp structure has anisotropic diffusion channels with fast oct–oct diffusion along the *c* axis[77].

It is hypothesized that although the 1D diffusion channels along the *c* axis in the hcp anion frameworks are fast, they may also be more prone to channel-blocking defects, often (but not always) resulting in a lower measured conductivity[76]. In fact, amongst crystalline halides with a close-packed anion sublattice, most of the reported halide solid-state electrolytes with high room-temperature ionic conductivity over 1 mS cm^{-1} possess the fcc structure[75]. Thus, effective structural regulation of close-packed structures is a method to improve ionic conductivity in close-packed halide structures. Specific examples are provided in the section where we discuss examples of superionic conductors.

Non-lithium cation frameworks. Owing to the lower screening power of O^{2-}, oxides require other mechanisms to be turned into fast Li-ion conductors. Indeed, none of the oxide-based lithium superionic conductors have a bcc anion framework, and the oxide analogues of sulfide-based superionic conductors show significantly higher activation energies[53,78,79]. This suggests that picking a preferred anion framework is not sufficient to achieve superionic conductivity in oxides where weak polarizability creates strong interactions between mobile Li ions and non-Li cations that dominate the energy along a migration path. Instead, enhancing Li mobility in oxides generally seems to be achieved with two guiding principles: minimize the repulsive interaction between Li and other cations by creating low-density structures or well-defined pathways where Li can stay away from the other cations, and/or increase the energy of Li sites so that they come closer to the energy of Li in the transition state. This can be done by distorting the Li sites or by introducing short-distance Li^+–Li^+ interactions achieved by stuffing materials with excess Li ions. In some materials, both principles can be at work.

An example of the first principle can be found in many fast Li-conducting oxides including NASICON[80], $LiTa_2PO_8$ (ref. 81) and $LiTaSiO_5$[82,83] where the framework formed by the non-Li cation polyhedra is only corner-sharing[51]. In such corner-sharing frameworks the non-Li cation polyhedra never share an edge or face with each other. Compared with non-corner-sharing frameworks, corner-sharing frameworks generally have a lower spatial density of non-Li cations, thereby maximizing the distance between Li and non-Li cations. This low cation number density is important as high-valent cations serve as high-energy repulsion centres that must be avoided by Li to migrate with low barrier. The sparse spatial distribution of non-Li cations in corner-sharing frameworks results in more favourable Li-ion diffusion channels that are minimally affected by non-Li cations (Fig. 2b). The second principle may also be at work in this family of materials as Li-ion sites tend to be highly distorted in corner-sharing frameworks, which is discussed in more detail in the next section. This corner-sharing framework feature is highly effective in rationalizing known oxide-based superionic conductors and discovering novel fast-conducting structural frameworks, among which $LiGa(SeO_3)_2$ was experimentally demonstrated to have a bulk ionic conductivity of 0.11 mS cm^{-1} at 300 K (ref. 51).

The benefit of maximizing the distance to other cations is well understood in layered materials, such as layered Li cathodes[84], in which a large interlayer spacing enables the Li-ion to maximize its distance from a transition metal as it passes through the activated state[85]. A similar idea is applied when designing superionic conductors. For example, in hcp-chlorine-packed trigonal Li_3YCl_6, a larger interlayer distance leads to a lower activation energy for in-plane Li-ion hopping[86] (Fig. 2c). In this system, Y^{3+} cations in the Li layer can serve as pillars to open up the interlayer space and promote in-plane Li-ion diffusion. Similarly, the large Ag^+ ion was introduced as a pillar into layered $Li_xAg_{1-x}CrS_2$ ($0 < x < 0.4$), which effectively improved its Li-ion conductivity up to 19.6 mS cm^{-1} (ref. 87). Because the interlayer distance between two anion planes results from a competition between the electrostatic attraction with the cations residing in between them and their steric repulsion to the anion, large low-valent cations are ideal as pillars to increase mobility of Li between two anion planes. Indeed, in some layered cathode materials, introduction of the smaller Ni^{2+} cation in the Li layer of $LiNiO_2$ has actually been shown to be detrimental to Li mobility[88] as it decreases the layer spacing.

Structural factors based on Li-ion site geometry and topology

Individual Li-ion coordination environments. While the cation and anion frameworks have important roles in determining the sites available for Li-ion diffusion and their connectivity, there are specific ways in which the Li-ion site energy can be modified to improve a material's ionic conductivity. Distortion of the Li-ion coordination geometry has been proposed as a mechanism to raise the Li-site energy, thereby lowering its migration energy (Fig. 3a, left). Destabilization of Li-ion sites via distortion does not need to impede the thermodynamic stability of a structure. Even raising the site energy by only a few hundreds of millielectronvolts can lead to a great improvement in conductivity, since at room temperature each 60-meV reduction in migration energy gives a tenfold increase in hopping rate if no changes to the prefactor are considered. Such small changes in site energy are negligible compared with the total binding energy of Li ions in oxides and sulfides, which is on the scale of several electronvolts[89,90].

A distorted coordination environment has been reported in various Li-ion conductors. For example, in $LiTi_2(PS_4)_3$ highly distorted Li-ion sites contribute to a flattening of the energy landscape[91]. In corner-sharing frameworks such as NASICON and $LiTa_2PO_8$, the Li coordination environment was found to be highly distorted, and the shapes of the Li polyhedra are not constrained by shared edges with more symmetric metal cation polyhedra[51].

Li-ion site energies can also be increased by forcing Li ions to occupy an unfavourable coordination environment. Li ions tend to prefer tetrahedral and octahedral coordination environments[92], which accounts for more than 80% of known Li-coordination environments observed in the ICSD database. An example of Li in an unfavourable coordination environment is in the perovskite superionic conductor $Li_{3x}La_{1/3-x}TiO_3$, where the relatively small Li^+ shares the same 12-coordinated dodecahedron site (A-site in perovskite, Fig. 3a, middle) with the large La^{3+}. Li ions are not well coordinated in such a large site, and neutron diffraction refinements[93,94] have shown that they tend to be bonded mainly to a specific facet of the dodecahedron.

One can also increase the energy of Li by increasing the size of its polyhedron[95]. Enlarged Li sites, as measured by Voronoi tessellation, are a common feature of prototypical superionic conductors, such as LLZO, LGPS and NASICON-type structures (Fig. 3a, right). The large site often leads to off-centring in the anion polyhedron and positional disordering of Li-ion sites, and is treated as split sites in Rietveld refinement of diffraction results. This feature of enlarged Li sites has been used to discover numerous other Li superionic conductors in oxide or sulfide chemistry[95].

Li stuffing. One very effective way to increase the energy of a Li ion in a host structure is to add so much Li that it starts to fill sites in close proximity to other filled Li sites. The Coulombic repulsion between Li ions raises their energy and enhances mobility. This is often referred to as 'Li stuffing' and can be achieved by

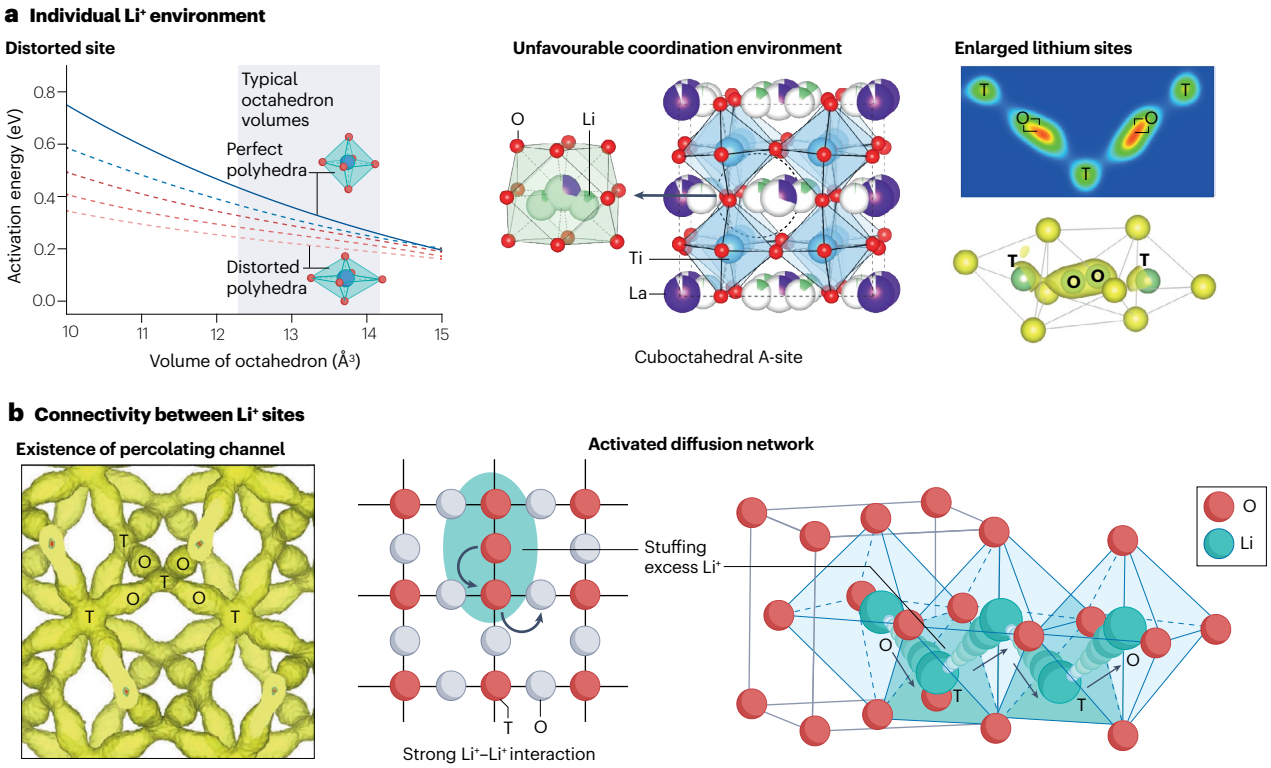

Fig. 3 | Features of Li-site topology in superionic conductors. a, Features of individual Li environments that benefit fast Li-ion diffusion. The left panel shows the effect of distorting the octahedral sites on the activation energy for a Li ion to escape the coordination environment[51] throughout a typical volume range (grey-shaded area). The middle panel shows a Li ion in perovskite-type $Li_{3x}La_{1/3-x}TiO_3$ occupying a highly unfavourable cuboctahedral A-site. The right panel shows an example of enlarged Li sites in garnet-type $Li_7La_3Zr_2O_{12}$, where Li ions occupy diffuse and large sites[95]. T and O indicate tetrahedral and octahedral sites. **b**, Common features related to the connectivity between Li sites include the existence of a percolating diffusion channel, preferably 3D[244], as well as an activated diffusion network. The left panel shows the Li probability analysis (yellow) calculated for garnet-type $Li_7La_3Zr_2O_{12}$ (ref. 244), which illustrates its 3D diffusion channels. The middle panel shows the effect of stuffing an excess Li into a diffusion network to form an activated diffusion network with strong local Li–Li interactions[100], such that Li can diffuse through the network with low barrier. Red and grey circles indicate occupied and unoccupied Li sites, and the green area indicates the activated local environment with strong repulsion between Li ions. The right panel shows concerted Li-ion hops as a result of strong Li interactions[104] in a close-packed oxide. Panel **a** left adapted from ref. 51, Springer Nature Limited. Panel **a** right adapted with permission from ref. 95, Wiley. Panel **b** left adapted from ref. 244, CC BY 4.0. Panel **b** middle adapted with permission from ref. 100, Wiley. Panel **b** right adapted from ref. 104, CC BY 4.0.

introducing off-stoichiometric excess Li via subvalent cation doping or substitution (such as $Ti^{4+} \rightarrow Al^{3+} + Li^+$).

Li stuffing has a highly nonlinear effect on the ionic conductivity because it does not just modify the carrier density, but also lowers the migration energy for Li hopping. With just a small amount of excess Li, the ionic conductivity is often improved by multiple orders of magnitude. For example, the bulk ionic conductivities of NASICON-type $LiZr_2(PO_4)_3$ and $LiTi_2(PO_4)_3$ improved by three orders of magnitude when increasing the Li content to $1 + x$ ($x = 0.3$) by subvalent cation substitution of the tetravalent cation[47,80,96,97]. Subsequent stuffing beyond $x > 0.3$ brings minimal improvement of ionic conductivity as it only increases the concentration of carriers[97,98]. A similar effect is observed in garnets. Although the well-known Li-garnet $Li_3Ln_3Te_2O_{12}$ (Ln = lanthanides) is a poor conductor with high activation energy, stuffed Li_{3+x} garnets show a much lower activation energy[99–103]. Even in rocksalt-like structures, which are typically poor conductors, only 10% Li over-stoichiometry leads to an improvement of four orders of magnitude in ionic conductivity[104,105]. This is why the majority of experimentally reported and computationally predicted superionic conductors contain off-stoichiometry. Hence, the effect of Li-stuffing on conductivity is non-traditional in that it does not just modify the carrier concentration (similar to doping a semiconductor with holes or electrons) but greatly lowers the activation energy.

For Li stuffing to turn a structure into a fast Li-ion conductor, specific topological criteria concerning the network of Li sites must be met. These are a 3D percolating diffusion network (Fig. 3b, left), short distances between occupied Li sites and sites where the extra Li goes (Fig. 3b, middle), and homogeneity of the transport path. Having short distances between Li sites ensures that when an excess Li is stuffed into a high-energy unoccupied site in the diffusion network, a strong Coulombic interaction is induced between the inserted Li and existing Li, creating a high mobility interstitial-like 'defect'. Homogeneity of the transport path guarantees that such an activated local environment (green region in Fig. 3b, middle) has symmetrically equivalent paths, preventing the excess Li from getting trapped in a low-energy state or blocked by a high-energy state. As such, the notion of stuffing excess Li to form activated diffusion networks goes beyond the textbook idea of generating defects to activate interstitial or interstitialcy diffusion.

While the benefits of Li stuffing are well known for garnet and NASICON-structured materials, similar results have now been observed in structures with an fcc O^{2-} framework, which generally were not thought to be particularly fast Li-ion conductors. In fcc anion frameworks, the presence of occupied face-sharing octahedra and tetrahedra creates strong repulsion, which leads to high ionic conductivity in both electrode materials[105,106] and conductors[104]. By stuffing excess Li into a rocksalt-type lattice, unique face-sharing Li configurations were created (Fig. 3b, right) and a σ_{300K} of 0.34 mS cm^{-1} could be achieved[104]. Similarly, in a high-throughput search for oxides with an activated diffusion network, a distorted inverse spinel structure with fcc O^{2-} packing Li_2TeO_4 was predicted to have a high σ_{300K} of 2.7 mS cm^{-1} when excess Li was introduced[100]. Therefore, inducing strong Li–Li interactions is a powerful mechanism to design superionic conductors.

Stuffed conductors may also benefit from what has been referred to as concerted, correlated or cooperative Li motion. Such phenomena have been reported in fast Li-ion conductors such as LGPS, LATP and LLZO[107], although they are sometimes imprecisely defined. Although these terms refer to similar phenomena, concerted motion specifically describes multiple Li-ions hopping within a single vibrational frequency (Fig. 3b, right), whereas correlated and cooperative motion refers to an initial hop triggering a subsequent hop to occur in close temporal proximity by lowering its migration barrier. The origin of these effects is the strong Li–Li interaction, which result in the concerted motion of Li ions when the hop of one Li causes another Li to no longer occupy a local energy minimum (site), forcing both Li ions to hop together. Therefore, temporally and spatially correlated Li-ion hops can be understood as a proxy for strong Li–Li interactions. The precise details of these mechanisms, as well as experimental methods to more rigorously detect them, are not well established yet.

In addition to Li stuffing, introducing Li off-stoichiometry via vacancy generation is a more conventional approach to improve ionic conductivity. Superionic conductors often show a balance of Li and vacancies within their diffusion channels. In materials where the initial Li content is high and Li-ion diffusion is facilitated by vacancies, introducing Li vacancies through aliovalent substitution of non-Li cations can substantially enhance the ionic conductivity. For instance, the low ionic conductivity observed in close-packed halides such as Li_2MCl_4 (for example, M = Mg) was theoretically demonstrated to be due to a low vacancy concentration[108]. In a subsequent investigation, a substantial improvement in ionic conductivity was achieved[109] by reducing the non-Li cation concentration to form $Li_2Sc_{2/3}Cl_4$. Similarly, in $Li_{3-x}M_{1-x}Zr_xCl_6$ (where M = Y, Er), the introduction of a small number of vacancies ($x = 0.2$) led to an order-of-magnitude enhancement in ionic conductivity[110].

Effect of rotationally mobile anion groups on Li-ion diffusion

Among fast Li-ion conductors, some structures have rotationally mobile anion groups (Fig. 4). The role of the rotational motion of anion groups in accelerating Li-ion transport has been termed the paddlewheel effect, cogwheel effect or revolving door mechanism. This mechanism was first proposed to connect the high ionic conductivity of high-temperature Li_2SO_4 (refs. 111–117) to the diffuse distribution of SO_4^{2-} groups in the framework. More recently, similar correlations between anion-group rotations and Li-ion diffusion have been claimed in various crystalline Li-ion conductors with PS_4, BH_4 and $B_{12}H_{12}$ groups[118–125].

Two types of rotational motion exist in inorganic materials. The first is librational motion (Fig. 4a), which is a vibration-like oscillation of the anion group as a rigid body around its local energy minimum. The second is large-angle rotation (such as 120°, Fig. 4b), where the anion group stochastically overcomes energy barriers to transition to another symmetrically equivalent orientation[126,127]. Although it is difficult to establish a spatially and temporally resolved correlation between such large-angle rotations and Li hopping, indirect evidence for a paddlewheel-like effect has been argued from the existence of rotational disorder observed in quasi-elastic neutron scattering[123,124,128–130], a maximum entropy analysis of neutron diffraction data[120,122] (Fig. 4e), and spin lattice relaxation NMR experiments[131,132]. In computational modelling, such correlations have been investigated using angular correlation functions[120,122], the Helmholtz free energy distribution[120,122], or a rotational version of the Green–Kubo formula[119]. Although these experimental and computational analyses suggest the existence of disordered anion-group orientations, they only provide time-averaged and space-averaged information, which cannot reveal the degree of correlation between rotational motion and Li-ion hops. Taking the

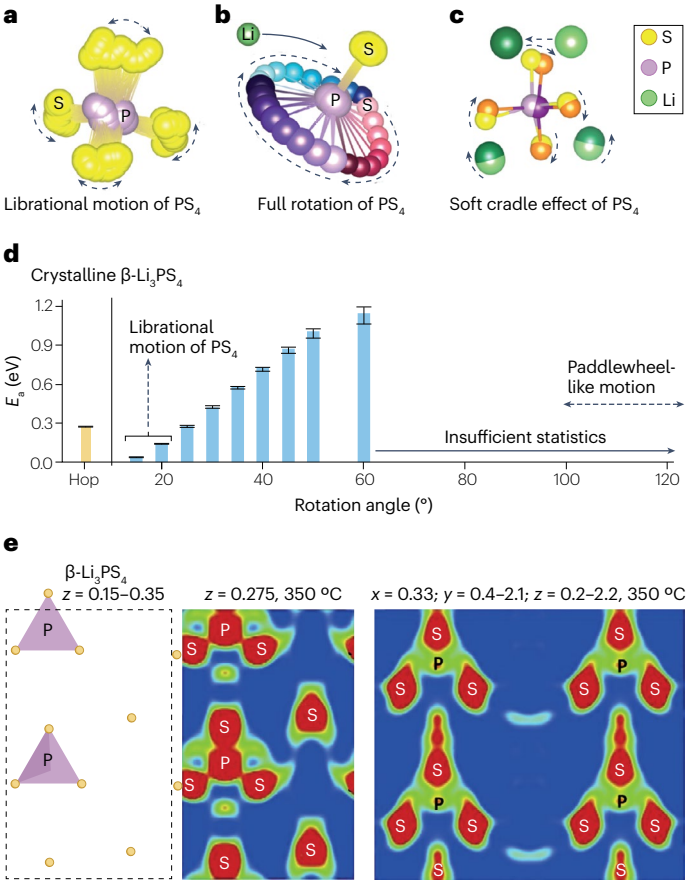

Fig. 4 | Effect of rotational motion of anion groups on Li-ion diffusion. **a**, Librational motion of anion groups. **b**, Paddlewheel-like motion with a full rotation of anion groups. The gradual increase in darkness for three S anions (pink, purple and blue) indicates the 120° rotational motion accompanied by a nearby Li-ion (green) hop. **c**, Li-hop-dependent tilting of anion groups (soft cradle effect). **d**, Activation energy of hop events (yellow) and rotation events of various angle cut-offs (blue) analysed from ab initio molecular dynamics trajectories of β-Li_3PS_4. **e**, Nuclear density plots computed by the maximum entropy method from neutron diffraction experiments on β-Li_3PS_4 at 350 °C (ref. 122). E_a, activation energy. Panels **a**–**d** adapted with permission from ref. 127, PNAS. Panel **e** reprinted with permission from ref. 122, Elsevier.

maximum entropy method as an example, the sulfur nuclear density plots (Fig. 4e) are averaged over trajectories during the neutron beam exposure time, therefore lacking the temporal and spatial resolution required to distinguish whether the signals originate from large-angle librational motion (or dynamic disorder) or static disorder. For this reason, they cannot serve as direct evidence for correlation between Li-transport and motion of anion groups.

Several papers have questioned whether there is a beneficial effect on Li-ion hopping from large-angle anion-group rotations[126,127]. A quaternion-based algorithm for detecting rotation events[127,133], which was applied to identify anion-group rotation and Li-ion hop events in the molecular dynamics trajectories of materials for which the paddlewheel effect has been claimed, showed that the activation energy of large-angle events is significantly higher than that of Li-ion hops (Fig. 4d). Moreover, the number of Li-ion hops that are temporally and spatially correlated with large-angle rotation is likely to be negligible at 300 K (ref. 127). Even small-angle librations of anion groups, although prevalent, were found to be uncoordinated with Li-ion hopping. Instead, a coordinated motion was observed in which the anion group may tilt its orientation to maintain optimal bonding with a migrating Li ion, essentially 'cradling' it to lower the transition state energy (Fig. 4c). Such an effect is pronounced only when anion groups are isolated without covalent bonds connecting them, which in fact corresponds to the materials for which the paddlewheel effect has been claimed. Thus, the soft-cradle effect can be understood as a mechanism by which ionic conductivity can be improved via the incorporation of weakly bound anion groups into the framework. The existence of such Li-occupancy-dependent tilting of anion groups was proved by various groups[119,126,127] and leads to static disorder of anion-group orientations whenever Li ions are disordered over their possible sites.

Anharmonic phonon modes that couple cation and anion motion have been suggested as a feature of materials with weakly bound anion groups. For example, inelastic neutron scattering and quasielastic neutron scattering experiments[134,135] in a Cu-ion conductor (argyrodite)[136] and in Na-ion conductors (Na_3PS_4) suggested that anharmonic low-energy phonon modes related to the local wiggling and translation of PS_4 groups positively benefit Na-ion diffusion by widening the bottleneck. Anharmonicity of a mode does not in itself improve Li-ion mobility, but an interaction whereby a Li-ion hopping mode and an anion-group mode favourably couple through anharmonicity would increase the hopping rate. Anharmonic phonon coupling calculations for ab initio molecular dynamics trajectories found that the anharmonic coupling of low-frequency Li phonon modes with high-frequency anion stretching and flexing modes may reduce the diffusion barrier[137].

To exploit the benefit of weakly bound anion groups, cluster-anion substitution on anion sites has been performed on various classes of conductors including Li-argyrodites[126,138–140], Li-antiperovskites[141] and Li-thiophosphates[142]. For example, a partial BH_4 substitution on the halogen site of Li_6PS_5Cl resulted in a σ_{300K} of 4.8 mS cm^{-1}. It was suggested that the weakened interactions between Li ions and BH_4 groups is responsible for the improvement of ionic conductivity. Computational work also showed that the responsive dynamics of BH_4 groups, which are conceptually similar to the soft-cradle effect, improve Li-ion conductivity[126].

Chemical factors for fast Li-ion diffusion

Although structural features of the crystal structure are the primary factor determining the properties desired in a superionic conductor, various chemical design strategies can be used to optimize the ionic conductivity achievable within the given structural space.

Effect of anion chemistry

As lithium ions reside in the coordination environment determined by the anion framework, the anion chemistry has a direct role in determining the achievable ionic conductivity within a given framework. More polarizable and larger anion chemistries, also referred to as soft anion sublattices, generally result in higher ionic conductivities and lower activation energies for two reasons (Fig. 5a). First, the energy well of each cation site is shallower in highly polarizable systems, resulting in a lower migration energy for Li ions to escape from initial sites. Second, more polarizable and larger anions have stronger screening power, minimizing the repulsion from non-Li cations. The larger distance between cations also leads to weaker cation interactions. This feature is often referred to as lattice softness[143–145].

The anion chemistry is the primary reason why ionic conductivity for a given structural prototype increases with row number in the periodic table, for example from oxides to sulfides to selenides. For example, whereas the oxide-LISICON has a low ionic conductivity of 0.001 mS cm^{-1} (ref. 146) at best, thio-LISICONs achieve superionic conductivity of up to 2.2 mS cm^{-1} (ref. 68). Similarly, a computational study showed that the oxide-analogue of LGPS has substantially lower ionic conductivity than LGPS[53]. Among halides, fluoride-based superionic conductors virtually do not exist, whereas for a given system, bromides tend to have higher ionic conductivity than chlorides[12]. It is noteworthy that although a softer lattice reduces the activation energy, it also reduces vibrational frequencies, leading to a smaller Arrhenius prefactor[147].

Effect of cation chemistry and disorder

Inductive effect. The cationic species within the framework influence the bond strength between Li ions and anions, a phenomenon often referred to as the inductive effect[148,149]. In a structure with a Li^+ ion, X^{n-} anion and A^{a+} non-Li cation, a more electronegative A^{a+} results in a lower charge density on the X^{n-} site (that is, less polar). As a result, the Coulombic interaction between the Li ion and X^{n-} becomes weaker, which reduces the binding energy of the Li ion to the X^{n-} anion and results in a lower barrier for Li-ion hops (Fig. 5b).

The inductive effect has been carefully studied for a given host framework with varying amounts of cation substitutions. For example, in the $Li_{10}GeP_2S_{12}$ system, gradual substitution of Ge to Sn was found to strengthen the Li–S bond, resulting in a higher activation energy[150,151]. A similar effect has been found in many other Li-conducting and Na-conducting systems, including NASICON-type $LiM_2(PO_4)_3$ (M = Zr, Sn)[152], $Na_{11}Sn_2PnS_{12}$ (Pn = P, Sb)[153] and $Na_3P_{1-x}As_xS_4$ (ref. 154). It is important to note that when introducing chemical substitution into a given framework, the inductive effect and the change in lattice volume may affect the ionic conductivity in opposite directions[151]. The role of the inductive effect on Li is secondary compared with that of the network topology and site energy discussed earlier, and should be thought of as a controllable but small lever to modify Li mobility.

Disorder between cations. More recently, the high-entropy concept has been introduced as a way to improve the ionic conductivity in a given framework[155,156]. The general idea is that the chemical disorder introduced by high-entropy mixtures will improve Li-ion conductivity. One specific mechanism by which high entropy operates is through the perturbation it generates on the Li-site energies, either

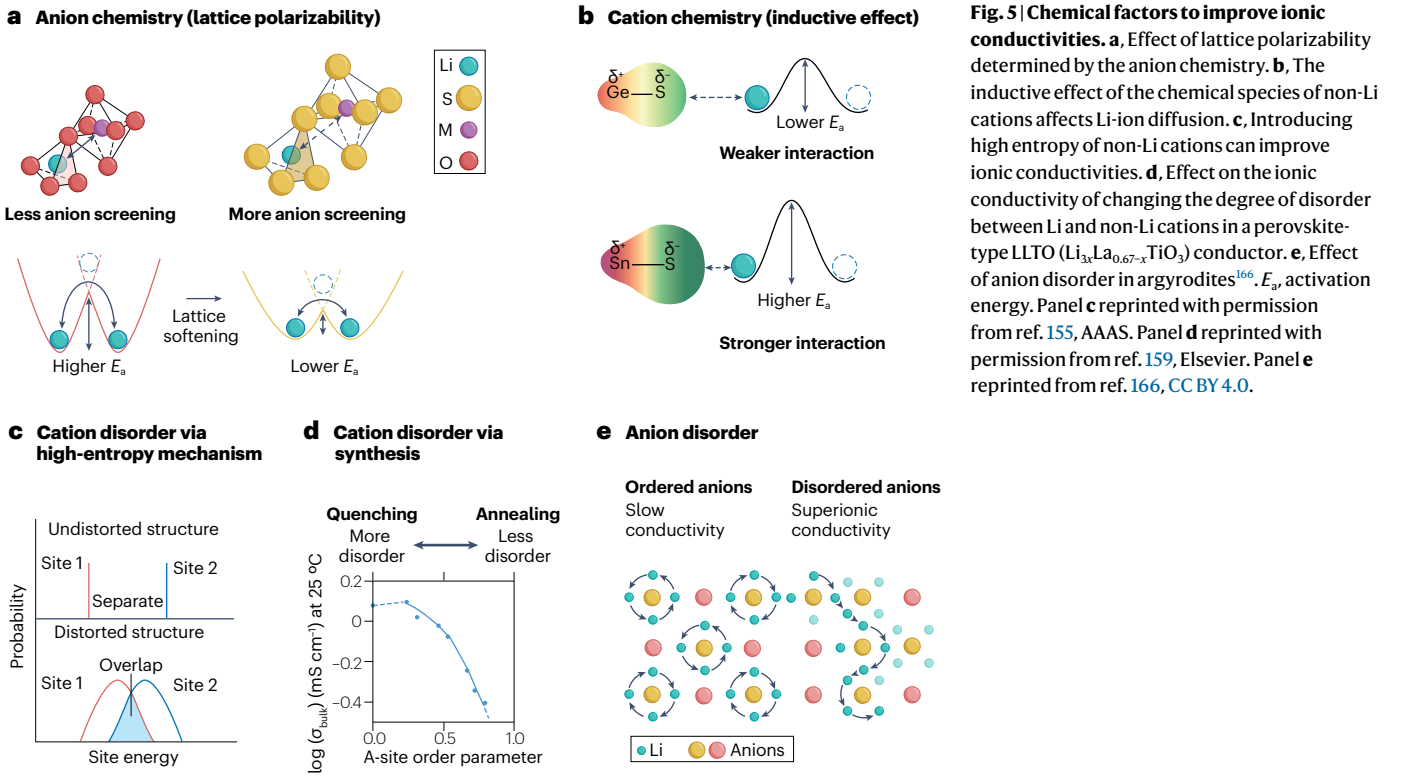

Fig. 5 | Chemical factors to improve ionic conductivities. a, Effect of lattice polarizability determined by the anion chemistry. **b**, The inductive effect of the chemical species of non-Li cations affects Li-ion diffusion. **c**, Introducing high entropy of non-Li cations can improve ionic conductivities. **d**, Effect on the ionic conductivity of changing the degree of disorder between Li and non-Li cations in a perovskite-type LLTO ($Li_{3x}La_{0.67-x}TiO_3$) conductor. **e**, Effect of anion disorder in argyrodites[166]. E_a, activation energy. Panel **c** reprinted with permission from ref. 155, AAAS. Panel **d** reprinted with permission from ref. 159, Elsevier. Panel **e** reprinted from ref. 166, CC BY 4.0.

through chemical bond effects as discussed previously, or through distortions arising from the different ionic size of the ions in the high-entropy mix. The broadening of the distribution of site energies can under certain circumstances lead to percolation pathways with lower average barrier. This is the case in structures, such as NASICONs, that have a variation in site energy along the Li migration path. Introducing high entropy can cause the energy distribution of these crystallographically distinct sites to overlap, creating a lower hopping barrier between them (Fig. 5c). If such neighbouring sites with small differences in site energy percolate, the Li-ion conductivity increases. In experiments, such broadening of Li-site energies is manifested as Li-site disorder in time-of-flight neutron diffraction patterns[155]. An improvement of σ_{300K} induced by high entropy has been demonstrated in Li-NASICON, Li-garnet and Na-NASICONs, and this strategy seems particularly effective in making poor conductors into better conductors[155]. An optimal degree of distortion from the high-entropy mechanism may exist, as an excessively broad site energy perturbation can limit percolation.

High-entropy cation disorder may also more directly improve Li-ion conductivity by destroying Li-vacancy ordering. This is expected to be particularly useful when a high-temperature Li-disordered state shows good conductivity, but Li-vacancy ordering quenches this conductivity at room temperature. While high entropy is an equilibrium approach to introduce more disorder, cation disorder can also be induced through materials processing, creating higher-energy states that are metastable at room temperature. Both ball-milling synthesis and high-temperature quenching fall into this category. An example of this is the optimization of perovskite-type $Li_{3x}La_{0.67-x}TiO_3$ (LLTO). In this compound, the A-site is shared between Li^+, La^{3+} and vacancies[157]. To circumvent the partially ordered state that is obtained when annealing at low temperature, quenching the material from high temperature can be used to achieve a high degree of disorder between the A-site cations[158]. The highest σ_{300K} is achieved when the A-site order parameter is lowest (more disorder)[159] (Fig. 5d). Strong A-site ordering upon annealing is accompanied by a phase transition from cubic to tetragonal perovskite, which has an alternating arrangement of La-rich and Li-rich layers along the *c* axis.

Mechanochemical synthesis (ball-milling) is another approach for introducing cation disorder in structures. The impact of cation disorder introduced this way is very prominent in close-packed crystalline halide conductors and has been extensively studied in recent years. A study[160] performed on the Li_3YCl_6 system demonstrated that mechanochemical synthesis introduces metastable transition metal cation disorder (and thereby superionic conductivity) into the structure. Subsequent annealing into a more thermodynamically favoured ordered phase results in an order-of-magnitude lower ionic conductivity. Li_3YCl_6 prepared via solid-state synthesis demonstrated the lowest degree of cation disorder and significantly lower σ_{300K} (3.4×10^{-2} mS cm^{-1}) compared with ball-milled Li_3YCl_6 (9.5×10^{-2} mS cm^{-1}). Similar trends in synthesis have been observed in Li_2ZrCl_6. Ball-milled Li_2ZrCl_6 has a σ_{300K} of 8.08×10^{-1} mS cm^{-1}, but this number drops by two orders of magnitude after annealing at 350 °C for 5 h (ref. 161). Today, most halide or oxyhalide Li-ion conductors with high Li-ion conductivity have been synthesized through extensive ball-milling[12,75,162,163], which may create a problem for the large-scale production of these materials. Ideally, cation disorder would be achieved with more scalable processing methods, or structures would be designed in which cation ordering does not negatively affect ionic conductivity.

Disorder between anions. Anion disorder has also been used as a strategy to improve ionic conductivity in inorganic crystalline materials (Fig. 5e). Anion disorder can be present when different anions occupy the same crystallographic site(s). In halogen-containing Li-argyrodites Li_6PS_5X (X = Cl, Br), S^{2-}, Cl^- and Br^- ions can share the same 4a/4c site, owing to their rather similar crystal radius (170 versus 167 versus 182 pm). The resulting anion disorder leads to a fourfold increase in the ionic conductivity (see next section)[164]. The amount of anion disorder can be tuned through synthesis temperature and then 'frozen in' via quenching[165]. Theoretical studies have shed some light on the mechanism by which anion disorder improves conductivity in the argyrodites[166]. In the anion-ordered Li_6PS_5X systems ($X = I^-$) with X^- occupying the 4a site and S^{2-} occupying the 4c site, Li ions are pseudo-ordered because of a shorter Li^+–S^{2-} bond than Li^+–X^- bond. This results in a specific part of the face-sharing tetrahedral network being higher in energy while the remaining channels near a 4c sulfur site show a cage-like local diffusion, thereby hampering long-range diffusion. When the anion sublattice is disordered as in Li_6PS_5X (X = Cl, Br), S^{2-} partially occupies both 4a and 4c sites, and the cages near 4a/4c sulfur sites start to geometrically overlap with each other and enable facile long-range diffusion. Similar to high entropy, anion disorder broadens the range of Li-site energies, enabling more low-energy migration pathways that connect the cages[165,166]. Introducing anion disorder was successful in other classes of superionic conductors as well, such as close-packed halides (such as $Li_3YBr_3Cl_3$)[167], LGPS-type structures (such as $Li_{9.54}Si_{1.75}P_{1.44}S_{11.7}Cl_{0.3}$)[168] and LZPS-type structures (such as $Li_{2.4}Zn_{0.25}PS_{3.9}Cl_{0.1}$)[169].

Development of fast diffusion in various classes of conductors

The mechanisms that we have discussed for enabling and enhancing superionic conductivity are rarely all present in a specific class of materials. In this section, we review the most important classes of superionic conductors and discuss how the aforementioned mechanisms contribute to their high ionic conductivity. We focus on Li-ion transport and refer the readers to other reviews for detailed information on other materials properties[12,98,170–175]. This discussion serves mostly as an illustration to understand the mechanisms at work in various conductor classes. For complete reviews of fast Li-ion conductors, we refer readers to other resources[12,72,75,98,162,170,173].

LISICONs/LGPS-type

The discovery of LISICON (Li superionic conductor) materials dates back to 1978 when Henry Hong identified $Li_{14}Zn(GeO_4)_4$ as the first LISICON electrolyte[79] (Fig. 6a). Much effort was then devoted to developing LISICON-type oxide electrolytes, but their ionic conductivity remained unsatisfying (10^{-4} mS cm^{-1}) at room temperature[79,176,177]. A substantial enhancement of ionic conductivity was achieved by substituting the oxygen skeleton with sulfur. In 2001, the thio-LISICON $Li_{3.25}Ge_{0.25}P_{0.75}S_4$, with a room-temperature conductivity of 2.2 mS cm^{-1}, was reported[78]. The larger ionic radius and polarizability of sulfur anions aid Li-ion migration but at the cost of high-voltage stability. The high ionic conductivity of thio-LISICON motivated elaborate exploration in the Li_4GeS_4–Li_3PS_4 system, which finally led to the identification of a new crystalline structure $Li_{10}GeP_2S_{12}$ (LGPS) in 2011 with an ultrahigh room-temperature ionic conductivity of 12 mS cm^{-1} (ref. 52).

One major factor that led to an order-of-magnitude improvement in ionic conductivity from thio-LISICON to LGPS is the anion framework. In thio-LISICONs, sulfur anions adopt an hcp configuration, whereas the sulfur anions in LGPS possess a more favourable bcc structure. To remove expensive Ge from this compound, LGPS systems with cation substitutions (including Sn, Si and Al) have been studied as alternatives[178–180]. In particular, the substitution of two elements for the Ge site was reported to enhance ionic conductivity by balancing a large lattice volume with high Li content[181,182]. In addition to double cation substitution, anion doping has also been used as an effective way to improve the conductivity. When introducing a small amount of Cl doping, the $Li_{9.54}Si_{1.75}P_{1.44}S_{11.7}Cl_{0.3}$ compound shows a high conductivity of 25 mS cm^{-1} with widely distributed 3D conduction pathways[168]. Inspired by the high-entropy design principle, in 2023, Ryoji Kanno and collaborators synthesized $Li_{9.54}[Si_{1-\delta}M_\delta]_{1.74}P_{1.44}S_{11.1}Br_{0.3}O_{0.6}$ (M = Ge, Sn) with a σ_{300K} of 32 mS cm^{-1} (ref. 183), remarkably high for an inorganic conductor. The compositional complexity creates highly disordered constituent anion species, which flatten the energy landscape, thus promoting Li migration.

NASICON-type

The NASICON (Na superionic conductor)-type framework is highly advantageous for fast Li-ion diffusion because of its corner-sharing framework, which minimizes the interaction between Li-ions and non-Li cations, and the naturally distorted Li-ion coordination environments that it provides. Na-NASICON conductors with the composition of $Na_{1+x}Zr_2P_{3-x}Si_xO_{12}$ were first reported by John Goodenough and collaborators in 1976 (ref. 184) (Fig. 6b). Li-based NASICONs including $LiZr_2(PO_4)_3$ (ref. 185), $LiTi_2(PO_4)_3$ (ref. 47) and $LiGe_2(PO_4)_3$ (ref. 186) were discovered subsequently, but their ionic conductivities are much lower than those of their sodium counterparts. Modifying the NASICON structure by Li stuffing has proved to be effective for improving ionic conductivity[47,96,97,187,188]. In Li-NASICONs, 6b (octahedral), 36f (tetrahedral) and 18e (octahedral) sites form a 3D oct–tet–oct face-sharing diffusion network. While the stoichiometric Li_1 NASICONs typically have full occupancy of 6b octahedral sites and vacancies in the remaining 36f/18e sites, stuffing excess Li into the diffusion network (Li_{1+x}) forms activated local environments with strong Li–Li interactions. Such activated local environments diffuse through the network with low barrier, resulting in orders-of-magnitude higher σ_{300K}. This is illustrated by Sc^{3+} doping in $LiTi_2(PO_4)_3$, which at the optimized composition $Li_{1.3}Sc_{0.3}Ti_{1.7}(PO_4)_3$ results in a room-temperature ionic conductivity of 4×10^{-1} mS cm^{-1}, two orders of magnitude higher than that of pristine $LiTi_2(PO_4)_3$ (1×10^{-3} mS cm^{-1})[80,188].

Among various cation dopants, aluminium results in the highest ionic conductivity[172], which is likely to be related to the strong inductive effect of Al on oxygen. This idea is confirmed by a systematic study conducted in 1990 on the conductivity of $LiTi_2(PO_4)_3$ using a series of M^{3+} dopants and showing that the highest total conductivity of 0.7 mS cm^{-1} was achieved for $Li_{1.3}Al_{0.3}Ti_{1.7}(PO_4)_3$ (LATP)[80]. To further increase the Li content, P^{5+} sites in LATP can be partly substituted by Si^{4+}. This co-doping strategy introduces a higher concentration of activated local environments, leading to a high ionic conductivity of 2 mS cm^{-1} in $Li_{1.7}Al_{0.3}Ti_{1.7}Si_{0.4}P_{2.6}O_{12}$ (refs. 189,190). High-entropy concepts can be applied towards boosting the conductivity of Li-based NASICONs without Li stuffing[155]. The high-entropy compound $Li(Ti,Zr,Sn,Hf)_2(PO_4)_3$ with no excess Li stuffing has an ionic conductivity of 2.2×10^{-2} mS cm^{-1}, which is one to two orders of magnitude higher than that of its single-metal analogue compounds.

Garnet-type

Garnet is the archetypal stuffed Li-ion conductor. Li-containing garnet was originally synthesized in 1969 as the cubic $Li_3La_3Te_2O_{12}$ (ref. 44)

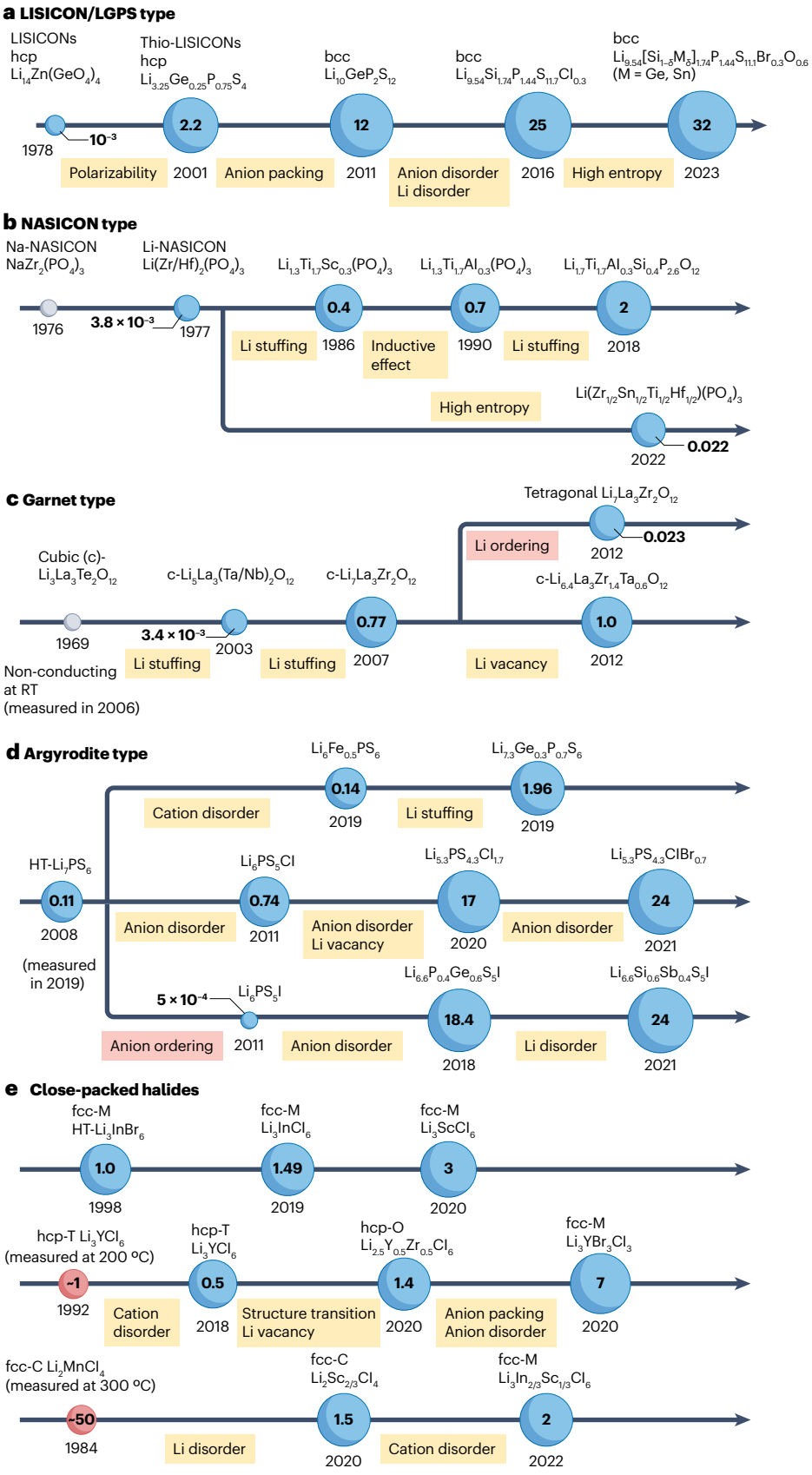

Fig. 6 | Breakthroughs in the enhancement of ionic conductivity using various design principles. Timeline of the main advances in LISICON/LGPS-type (panel **a**), NASICON-type (panel **b**), garnet-type (panel **c**), argyrodite-type (panel **d**) and close-packed halide (panel **e**) electrolytes. The size of each circle is proportional to the log of the total conductivity, σ_{300K}, which is indicated inside each circle (units mS cm^{-1}). Blue circles represent the total ionic conductivity at 300 K. Red circles indicate ionic conductivities measured at elevated temperatures because they are too low to be measured at 300 K. Grey circles represent unmeasured ionic conductivity or non-Li-ion conductors. Yellow text indicates the mechanisms at work to improve ionic conductivity, whereas red text indicates factors that lead to decreased ionic conductivities. Close-packed halides are labelled in panel **e** by their anion framework (hexagonal close packed, hcp; or face-centred cubic, fcc) and symmetry (C = cubic, M = monoclinic, T = trigonal, O = orthorhombic). bcc, body-centred cubic; LGPS, $Li_{10}GeP_2S_{12}$; RT, room temperature.

(Fig. 6c). However, it was not until 2003 that garnets became promising superionic conductors, when Venkataraman Thangadurai and collaborators discovered Li-stuffed $Li_{3+2}La_3M_2O_{12}$ (M = Ta or Nb) with a σ_{300K} of ~10^{-3} mS cm^{-1} (ref. 45). Subsequent research has revealed that a low activation energy can be achieved when $x > 0$ in $Li_{3+x}La_3M_2O_{12}$ (refs. 99–101,191). In 2007, the cubic-structured $Li_7La_3Zr_2O_{12}$ was reported, featuring a high conductivity of 7.74×10^{-1} mS cm^{-1} and low activation barrier of 0.3 eV (ref. 48), although this compound probably had a small amount of Al-doping from the Al_2O_3 crucible that led to the stabilization of the cubic phase[192,193]. Further tuning the Li content with cation doping resulted in the optimized cubic-structured compound $Li_{6.4}La_3Zr_{1.4}Ta_{0.6}O_{12}$, with a conductivity of 1 mS cm^{-1} (ref. 46).

The evolution of garnets as conductors beautifully illustrates how a diffusion network can be activated by Li-stuffing. In cubic garnet, the 24I tetrahedral and 48g/96h octahedral sites face-share with one another, creating a 3D network of tet–oct–tet configurations (Fig. 3b). In Li_3 phases, all Li ions occupy the 24d tetrahedral sites. However, in Li-stuffed garnets (Li_{3+x} phases), Li ions are highly disordered over both tetrahedral and octahedral sites, leading to a large number of face-sharing tet–oct environments[194,195]. These higher-energy environments can propagate through the network with low migration barrier. In ab initio molecular dynamics simulations of $Li_7La_3Zr_2O_{12}$, even concerted migration of Li ions has been observed, where the hopping of tetrahedral Li ions triggers the hopping of octahedral Li ions into neighbouring tetrahedral sites[107,196].

The degree of Li-vacancy ordering has an important role in influencing the ionic conductivity of garnets. A tetragonal $Li_7La_3Zr_2O_{12}$ polymorph can be obtained when synthesized without dopants such as Al or Ta (ref. 197). In contrast to the highly disordered Li distribution in cubic garnets, the Li sites in tetragonal garnets are fully ordered, with tetrahedral Li sites being completely filled, which is unfavourable for tet–oct–tet diffusion. The highest ionic conductivity reported for tetragonal-phase $Li_7La_3Zr_2O_{12}$ is 2.3×10^{-2} mS cm^{-1}, two orders of magnitude lower than that of the cubic polymorph[198].

Argyrodite-type

The Li-argyrodite structure is among the fastest inorganic conductors with intrinsically favourable 3D diffusion channels of face-sharing tetrahedral sites[72]. The stoichiometric Li-argyrodite Li_7PS_6 was first reported by Hans-Jörg Deiseroth and collaborators in 2008 (ref. 199) (Fig. 6d). This material has a low-temperature orthorhombic polymorph and a high-temperature cubic polymorph[200], with high-temperature Li_7PS_6 displaying the higher ionic conductivity[201]. High-temperature Li_7PS_6 has been stabilized at 300 K in 2019 using anhydrous ethanol-based wet chemical methods and has a σ_{300K} of 0.11 mS cm^{-1} (ref. 202). Chemical substitution on both the anion and cation lattice has been a common strategy to increase the σ_{300K} of Li-argyrodites, which can now be as high as 24 mS cm^{-1} (refs. 203,204). Early chemical substitution focused on the partial substitution of the S^{2-} that is not bonded in the PS_4 group with halogens Cl^-, Br^- and I^-, resulting in a mixed-anion structure Li_6PS_5X (X = Cl, Br, I). In 2011, Li_6PS_5X was synthesized via ball-milling, reaching ionic conductivities of 0.74, 0.72 and 4.6×10^{-4} mS cm^{-1} for X = Cl, Br, and I, respectively[164]. Partial anion substitution stabilizes the high-temperature cubic polymorph of Li_7PS_6 with substantial S^{2-}/X^- (X = Cl, Br) anion disorder, which is believed to promote Li^+ mobility in the structure[205]. The lower ionic conductivity of Li_6PS_5I is explained by the fact that it shows no anion disorder, probably owing to the larger ionic radius of I^- compared with S^{2-}. It should be noted that substitution of S^{2-} by X^- also introduces Li vacancies, which are also likely to enhance Li mobility. In 2020, increasing the Li off-stoichiometry via further substitution of S^{2-} by Cl^- or Br^- led to a fourfold increase in ionic conductivity from pristine Li_6PS_5X, achieving 17 mS cm^{-1} in $Li_{5.3}PS_{4.3}Cl_{1.7}$ and 4.35 mS cm^{-1} in $Li_{5.5}PS_{4.5}Br_{1.5}$ (refs. 206,207). Many other stoichiometries of Li-deficient argyrodites $Li_{6-x}PS_{5-x}Cl_{1+x}$ have also been investigated, with similar success[208,209]. In this space, mixed-halogen substitution in $Li_{5.3}PS_{4.3}ClBr_{0.7}$ has so far achieved a high ionic conductivity of 24 mS cm^{-1} (ref. 203), with disorder between Cl^-, Br^- and S^{2-} sites.

Aliovalent cation substitution of Li^+ for higher-valence cations Fe^{2+}, Ca^{2+}, Al^{3+}, Si^{4+} and Ge^{4+} has also been shown to enhance Li-ion conductivity[210]. In 2019, partial Li^+ substitution by Fe^{2+} to $Li_{7-2x}Fe_xPS_6$ resulted in an ionic conductivity of 0.14 mS cm^{-1} at $x = 0.5$ and in the stabilization of the high-temperature cubic phase at room temperature[211]. When combining anion disorder with aliovalent doping, one observes increased Li off-stoichiometry, Li-cation site disorder and ionic conductivity. In 2020, $Li_{5.4}Al_{0.2}PS_5Br$ was shown to exhibit a conductivity of 2.4 mS cm^{-1}, a threefold increase over pristine Li_6PS_5Br (ref. 210). Finally, rather than substituting S^{2-} or Li^+ in argyrodites, one can also substitute P^{5+} with Si^{4+} or Ge^{4+} to stabilize the high-temperature cubic structure, leading to ionic conductivities of up to 2.4 mS cm^{-1} for $Li_{6.5}P_{0.5}Si_{0.5}S_5Br$ and 1.96 mS cm^{-1} for $Li_{7.3}Ge_{0.3}P_{0.7}S_6$ (refs. 212,213). Ge^{4+} and Si^{4+} increase conductivity more than Sn^{4+}, owing to the inductive effect leading to lower bonding strength between Li^+ and S^{2-} (ref. 150). Some of these results show that even without anion disorder, significant disorder in the Li sublattice can result in high ionic conductivity, up to 3 mS cm^{-1} in $Li_{7.3}Si_{0.33}P_{0.67}S_6$ (ref. 214). On introducing excess Li into the structure, Li begins to occupy high-energy interstitial sites, which can lead to concerted ion migration and a lowering of the migration energy barrier[72].

Aliovalent substitution in Li_6PS_5I, in which anions are ordered, can induce anion disorder between S^{2-} and I^-, leading to a great increase in ionic conductivity. This was strikingly shown in 2018 with $Li_{6.6}P_{0.4}Ge_{0.6}S_5I$, which has a cold-pressed ionic conductivity of 5.4 mS cm^{-1}, and of 18.4 mS cm^{-1} on sintering, four orders of magnitude higher than that of pristine, anion-ordered Li_6PS_5I (ref. 215). By replacing P^{5+} with Sb^{5+} and using Li off-stoichiometry with Si^{4+}, concerted ion motion, and anion disorder, $Li_{6.6}Si_{0.6}Sb_{0.4}S_5I$ reached a high conductivity of 14.8 mS cm^{-1} when cold-pressed and of 24 mS cm^{-1} after sintering[204].

Close-packed halides

Fast-conducting halides typically contain group 3 cations (Sc, Y, La–Lu) or group 13 cations (Al, Ga, In) and have either hcp or fcc anion packing. Ordering of the metal and Li cations over the interstitial sites in these anion packings then further reduces the symmetry. Common symmetries are trigonal ($P\bar{3}m1$) and orthorhombic (*Pnma*) for the hcp anion sublattice, and monoclinic (*C2/m*) or cubic ($Fd\bar{3}m$) for the fcc anion sublattice. Both anion and cation arrangements are important for Li-ion conductivity: the anion sublattice determines the connectivity of the interstitial sites and the coordination changes encountered when the Li ion migrates[76], and the cation ordering controls which sites in the network are available and, through the electrostatics[86], the migration barrier in these sites.

Many improvements in close-packed halide conductors are a result of chemical modifications or synthesis methods that induce a structural change to a different anion packing and/or modify cation ordering. Figure 6e illustrates how different close-packed halides classified by their starting structures (fcc-monoclinic, fcc-cubic or hcp-trigonal) have been optimized. In every branch, *C2/m* monoclinic (fcc) halides have the highest ionic conductivity, owing to their

isotropic diffusion network, and the *Pnma* orthorhombic structure tends to have higher ionic conductivity than the trigonal structure, owing to an increased number of diffusion pathways in *Pnma* cation arrangements[77]. Although ternary bromides and iodides crystallize in the monoclinic *C2/m* structure and typically have higher ionic conductivity than chlorides[12,75], they are not studied as systematically due to their lower electrochemical stability window (~4 V for chlorides versus ~3 V for bromides)[76]. Thus, we primarily focus on improvements in the ionic conductivity of ternary metal chlorides. Fluorides are also not considered here, owing to their lacklustre ionic conductivity.

Crystalline halide solid-state electrolytes with a close-packed anion framework and metal components ($Li_aM_bX_c$, M = Mn, In, Y and so on) were initially reported in the 1970s to 1990s with measured ionic conductivities of 1–10 mS cm^{-1} at temperatures between 200 and 400 °C (refs. 216,217). In 2018, Tetsuya Asano and collaborators[218] discovered that hcp-anion-packed halides Li_3YCl_6 with trigonal symmetry are superionic conductors with a σ_{300K} of 0.5 mS cm^{-1} when created through mechanochemical synthesis (ball-milling). This work spurred extensive research in the chloride chemistry for fast Li-ion conductors. Ball-milling was shown to greatly improve the ionic conductivity in trigonal Li_3YCl_6 by introducing M^{3+}/vacancy disorder[160]. Aliovalent substitution of Y^{3+} by Zr^{4+} creates the orthorhombic *Pnma* structure (hcp) in $Li_{3-x}Y_{1-x}Zr_xCl_6$. Optimizing the substitution level enabled a conductivity of 1.4 mS cm^{-1} for $x = 0.5$ (ref. 110). Structural changes have also been achieved in trigonal halides by isovalent doping, which can alter the anion sublattice depending on the radii and polarizability of the introduced cation[219,220]. The synthesis of a series of $Li_3Y_{1-x}In_xCl_6$ conductors ($0 \leq x < 1$) showed that the ionic conductivity rapidly increases when the material transitions from the trigonal phase with hcp anion sublattice (0.067 mS cm^{-1}, $x = 0.1$) to the monoclinic (*C2/m*) phase with the fcc anion sublattice (0.60 mS cm^{-1}, $x = 0.2$)[221]. A similar ionic conductivity improvement accompanied by a transition from trigonal (hcp) Li_2ZrCl_6 to monoclinic (fcc) $Li_{2+x}Zr_{1-x}In_xCl_6$ was observed[222], although the change in Li concentration may have played an important role as well. In fact, when the composition is fixed at Li_2ZrCl_6, Li_2ZrCl_6 shows the opposite trend, as the transformation from hcp to fcc upon heat treatment results in a reduction of ionic conductivity by two orders of magnitude[161,223]. The highest ionic conductivity for close-packed halides has been reported for a mixed-halide $Li_3YBr_3Cl_3$ conductor, with an ionic conductivity of 7 mS cm^{-1} (ref. 167). In addition to benefiting from its monoclinic phase, $Li_3YBr_3Cl_3$ contains a significant amount of Li in tetrahedral sites, which lowers the migration energy barrier in close-packed halides owing to their higher site energy[76]. Improved grain contact achieved with hot pressing is also likely to have contributed to the high conductivity of the material. Finally, proper balancing of the pillar effect and the Li-ion percolation pathways led to a substantial increase in the ionic conductivity of hcp-chlorine-packed trigonal halides. In 2023, hcp-chlorine-packed $Li_3Y_{0.2}Zr_{0.6}Cl_6$ was synthesized by doping the trigonal Li_3YCl_6 structure with Zr^{4+} to introduce cation deficiencies, which create percolation channels while maintaining enough cation density to increase the interlayer spacing[86]. The $Li_3Y_{0.2}Zr_{0.6}Cl_6$ composition has a σ_{300K} of 1.19 mS cm^{-1}, a twofold increase over pure Li_3YCl_6 (0.5 mS cm^{-1}).

Notably, in 1998, another class of *C2/m* monoclinic close-packed halide with fcc anion packing was discovered. The high-temperature phase of Li_3InBr_6 with *C2/m* monoclinic symmetry and fcc anion packing was stabilized at 300 K using solid-state synthesis to achieve $\sigma_{300K} > 1$ mS cm^{-1} (ref. 224). Although the fast-conducting high-temperature phase could not be sustained at lower temperature (−13 °C), this work demonstrated that high Li-ion conductivity might be possible in halides. Subsequently, in 2019, an isostructural chloride (fcc, *C2/m* monoclinic) with group 13 cation Li_3InCl_6 was reported to have a σ_{300K} of 1.49 mS cm^{-1} (ref. 225) with the advantage that it could be synthesized in air without ball-milling. The structure is a distorted rock-salt LiCl structure with a high concentration of intrinsic vacancies, which is hypothesized to be the reason for its high conductivity. The highest ionic conductivity among the close-packed chloride family was achieved in Li_3ScCl_6 (*C2/m* monoclinic, isostructural to Li_3InCl_6), with a σ_{300K} of 3.02 mS cm^{-1} (ref. 226).

In 2020, a new family of close-packed superionic conductors with a group 13 cation $Li_2Sc_{2/3}Cl_4$ was synthesized through a solid-state method with a σ_{300K} of 1.5 mS cm^{-1} (ref. 109). $Li_2Sc_{2/3}Cl_4$ is a polymorph of the previously discussed *C2/m* Li_3ScCl_6 but with a disordered spinel structure similar to the cubic inverse spinel structures of the divalent metal halides studied in the 1980s ($Li_{2-2x}M_{1+x}Cl_4$ (M = Mn, V, Fe, Cd, Mg)) and has a fcc anion framework within the $Fd\bar{3}m$ cubic symmetry[227]. Although also a spinel, $Li_2Sc_{2/3}Cl_4$ contains a highly disordered distribution of Li, with four types of Li sites in both tetrahedral and octahedral environments, as opposed to the two types of sites in the previously slow-conducting inverse spinel structure[109]. Recently, isovalent doping by In^{3+} was used in this material to induce a cubic to *C2/m* monoclinic phase transition, leading to an improved σ_{300K} of 2 mS cm^{-1} in $Li_3In_{2/3}Sc_{1/3}Cl_6$ (ref. 11).

There are two limitations to the continued advancements in close-packed halides. First, the range of synthetic methods by which well-conducting crystalline halides are created has so far been limited. Many of them are synthesized through extensive ball-milling either to achieve a desired composition that is metastable and unreachable through more standard techniques, or to bypass metal ordering, which can quench the conductivity. A better understanding of the relation between equilibrium metal ordering, composition and conductivity is needed to move away from ball-milled materials. Whether such a synthesis technique is viable for large-scale application in the battery industry remains unclear. Second, the ionic conductivities of close-packed chloride conductors seem to have reached an upper limit[228], with the ionic conductivities failing to surpass 3 mS cm^{-1}. This upper limit may originate from their activation energy being bound by the relatively high intrinsic hopping barrier of close-packed halide frameworks as well as from their highly symmetric Li-coordination environments[76].

Other notable superionic conductors

Several other classes of materials show superionic conductivity. Among the sulfides, α-Li_3PS_4 has a mixed 75%/25% bcc/hcp character, allowing it to achieve higher ionic conductivity than the 100% hcp-packed Li_3PS_4 polymorphs[56]. In addition, the soft-cradle effect has been identified in both α-Li_3PS_4 and β-Li_3PS_4 to improve ionic mobility[127]. $Li_7P_3S_{11}$ is another example of a bcc-framework superionic conductor[50]. Among the oxides, $LiTa_2PO_8$ and $LiTaSiO_5$ both show strong resemblance to NASICON-type structures[51], with corner-sharing octahedra and tetrahedra, as well as highly distorted Li coordination environments. Their conductivities improve upon Li-stuffing as well[229]. Over-stoichiometric rocksalt-type oxides (such as $Li_{17}In_9SnO_{24}$) have recently been reported as a new group of Li superionic conductors in which face-sharing Li configurations aid ionic conduction considerably[104].

Whereas the family of close-packed chlorides seems to be limited to an ionic conductivity of a few milliSiemens per centimetre at room temperature, non-close-packed chlorides or oxychlorides may have

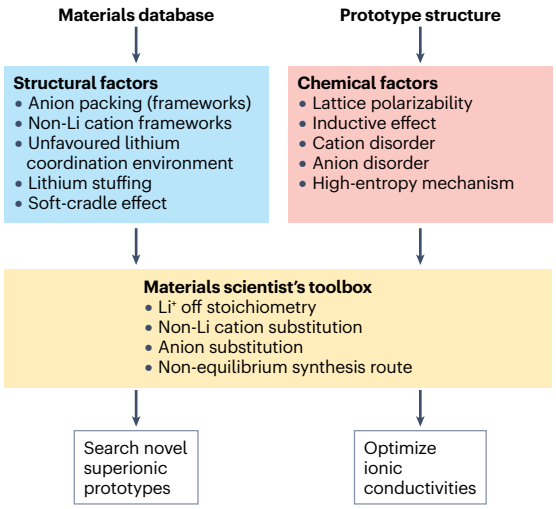

Fig. 7 | Design strategies for superionic conductors. Various structural features (blue) are used to discover new superionic prototypes from materials databases such as the Materials Project[245], whereas chemical features (pink) are often used to optimize ionic conductivities of a given prototype structure. Experimental and computational handles can be used to improve ionic conductivities by optimizing these structural and chemical factors.

higher ionic conductivities. For example, $LiTaOCl_4$ and $LiNbOCl_4$ have conductivities of 12.4 mS cm^{-1} and 10.4 mS cm^{-1} (ref. 163), respectively. It was suggested that this framework of 1D bonded octahedra is rotationally flexible and show the soft-cradle effect[230,231]. In addition, it shares the benefits of corner-sharing frameworks. Li-stuffed $LaCl_3$-type materials are another example of non-close-packed chlorides that provide high Li-ion conductivity. Here, Li stuffing was found to expand the dimensionality of diffusion channels from 1D to 3D[232]. Higher-dimensional diffusion channels are practically required, as materials with 1D diffusion channels are susceptible to channel blockage issues due to unavoidable point defects[233].

Outlook and future perspectives

We have discussed multiple atomic-scale mechanisms that can lead to high Li-ion conductivity in various materials classes. Almost all fast Li-ion conductors benefit from one or more of these mechanisms, although not all have to present in a single material. It is also not clear to what extent the various mechanisms augment each other (for example, Li-stuffing and high-entropy cations). What is remarkable is that, in many cases, application of these design principles can make a very poor structure into a highly conducting one (as for garnets). This suggests that a plethora of underexplored, seemingly mediocre conductors are awaiting discovery and transformation into superionic conductors.

The insights presented in this Review may not only accelerate the discovery of new prototype structures with desirable structural features but also provide avenues to optimize the ionic conductivities of known prototypes using diverse chemical factors (Fig. 7). Researchers can use the material scientist's toolbox to harness these advantageous structural and chemical factors. The dual approach of uncovering novel prototypes and refining known ones may ultimately lead to the development of a superionic conductor that satisfies all the practical criteria required for a solid electrolyte, which, besides high conductivity, include factors such as cost, processability, chemical and electrochemical stability, and appropriate mechanical properties.

There is much complementarity between computational and experimental approaches due to the different length scales and timescales at which they evaluate conductivity. For the same reason, there is also much work left for each field to help to validate and support the other. So far, computational work has mostly contributed to the understanding of atomistic diffusion mechanisms within the bulk, extraction of common features of fast ion conductors, rationalization of hypotheses on factors that may or may not improve ionic conductivity, and the discovery of new fast-conducting frameworks. Meanwhile, experimental evaluation of materials typically measures the overall conductivity of a macroscopic sample, which includes all the complexities from synthesis, grain boundaries and densification, and defect issues or second phases that may be challenging to characterize. Because ionic conductivity is not an 'averaged' property but is determined by the fastest path through a sample, small imperfections such as a grain boundary phase or low-density region, or other blocking defect, can contribute disproportionately to the measured conductivity. These challenges can make the direct comparison between theoretical and experimental work frustrating.

To alleviate the bottleneck of experimental realization of predicted superionic conductors, extra measures must be taken to bridge the gap between computational predictions and experimental attempts. Thus, it is of particular importance to extend state-of-the-art computational tools and machine-learning methods to provide insights in not only the bulk ionic conductivity, but also other experimental factors that make the development process challenging. Some of the required insights include elucidating grain boundary diffusion, predicting potential synthesis routes for new candidate materials, evaluating finite-temperature phase stability and phase competition, and predicting stability in atmosphere or humid air. In addition, going beyond the conventional Nernst–Einstein relationship to quantify correlation factors in the motion of various species is essential to improving the prediction of ionic conductivities using computational methods. That includes the degree of correlation between distinct Li-ions (so-called correlated or concerted motion) and the correlation between anion-group rotations and Li-ion hops. As it is extremely challenging to get direct mechanistic evidence of correlative motion using experimental methods, we believe that precise statistical analyses to understand the joint probability of Li-ion hops, the rotational motion of anion groups[127], the translation motion of non-Li cations, and the translational motion of anions must be conducted. Finally, the issue that σ_{300K} predictions in ab initio molecular dynamics are achieved by an Arrhenius extrapolation from high temperature, and may therefore miss deviations from Li-vacancy ordering[234] or the convolution of multiple pathways with very different activation energy[18], may ultimately be resolved with the recent introduction of machine-learning interatomic potentials, especially fine-tuned for each system[101,235].

From an experimental perspective, sustained endeavours are necessary to validate computational hypotheses and provide new mechanistic insights. Such insights require a comprehensive picture that correlates the structural features both at long and local range to ion transport across a wide range of scales. In this regard, advanced characterization techniques that can capture those structural features and probe ion diffusion at distinct timescales and length scales are highly demanded. From the structural perspective, the defects and disorder commonly involved in superionic conductors render classical crystallography tools based on perfect periodicity (such as diffraction)

inadequate. Techniques such as diffuse scattering, solid-state NMR, X-ray absorption spectroscopy, and scanning transmission electron microscopy need to be combined to characterize local structural features. In addition, the development of advanced characterization techniques with improved spatial or temporal resolution is particularly critical for ionic conductors, as it would open up opportunities to capture structural heterogeneities and dynamics that cannot be attained by conventional techniques with time-averaged and/or spatially averaged information. From the ion diffusion perspective, combining techniques that probe microscopic and macroscopic ion diffusion is essential to yield a complete picture of ion transport in crystalline materials. It is important to understand and specify the timescales and length scales of each probing technique and their limitations, enabling precise and rigorous comparison. Advanced techniques that can directly probe a material's intrinsic ionic conductivity without grain boundary, interface and porosity effects (such as individual particle conductivity measurements)[236] would be particularly promising. Such advancements could greatly accelerate materials screening for ionic conductors by bypassing time-consuming processing engineering when validating a new material.

The design principles that we have discussed have led to numerous computationally predicted fast ionic conductors[51,95,100,237,238], with only a small portion of them experimentally verified. This lack of integration between theory and experiment is because of the intrinsic challenges encountered during the experimental development of a new ionic conductor. Finding the optimal synthesis recipes to form thermodynamically metastable materials can be challenging and time-consuming. Furthermore, achieving the desired ion-conducting properties requires more than just attaining the correct long-range ordering. Local defects and disorder also need to be carefully regulated, which makes the synthesis even more complicated. Thus, it is essential to explore non-equilibrium synthetic pathways such as solution synthesis for metastable phases[63], high-energy ball-milling to create defects and disorder[239], and quenching from high temperature to kinetically stabilize polymorphs[240]. Mechanistic understanding of how such synthesis techniques lead to a specific non-equilibrium structure would greatly accelerate the overall design and development process of new conductors.

Understanding phase formation mechanisms and reaction pathways or seeking ways to thermodynamically stabilize the desired structures by both experimental and computational studies is essential for rationally designing synthesis routes. Autonomous synthesis laboratories can greatly accelerate materials discovery[241–243], although for many classes of conductors they will have to be able to handle very air-sensitive materials. In addition to synthesis, optimizing the densification process with desirable sintering conditions for EIS measurements is crucial to verify the predicted ionic conductivity, which is particularly important for oxides with low mechanical deformability.

As this Review clearly suggests, there is no single universal mechanism by which fast Li-ion diffusion can be activated. In addition, having one feature common in typical superionic conductors does not guarantee high ionic conductivity. Each class of materials has its own set of unique features that lead to its state-of-the-art ionic conductivity. This means that multiple design principles can be assembled to optimize a given class of materials towards higher ionic conductivity. Moreover, it is likely that the set of design principles outlined in this Review is incomplete and that new insights will generate even more opportunities. The diversity of handles by which to improve ionic conductivity suggests ample room for experimental and theoretical work in designing new fast Li-ion crystalline superionic conductors.

Published online: 12 September 2024

References

1. Janek, J. & Zeier, W. G. A solid future for battery development. *Nat. Energy* **1**, 16141 (2016).
2. Wang, C. & Sun, X. The promise of solid-state batteries for safe and reliable energy storage. *Engineering* **21**, 32–35 (2023).
3. Wang, R., Cui, W., Chu, F. & Wu, F. Lithium metal anodes: present and future. *J. Energy Chem.* **48**, 145–159 (2020).
4. Cheng, D. et al. Manufacturing scale-up of anodeless solid-state lithium thin-film batteries for high volumetric energy density applications. *ACS Energy Lett.* https://doi.org/10.1021/acsenergylett.3c01839 (2023).
5. Zhao, Q., Stalin, S., Zhao, C.-Z. & Archer, L. A. Designing solid-state electrolytes for safe, energy-dense batteries. *Nat. Rev. Mater.* **5**, 229–252 (2020).
6. Salamon, M. B. *Physics of Superionic Conductors* 175–199 (Springer, 2011).
7. Dieterich, W., Fulde, P. & Peschel, I. Theoretical models for superionic conductors. *Adv. Phys.* **29**, 527–605 (1980).
8. Diederichsen, K. M., McShane, E. J. & McCloskey, B. D. Promising routes to a high Li^+ transference number electrolyte for lithium ion batteries. *ACS Energy Lett.* **2**, 2563–2575 (2017).
9. Choo, Y., Halat, D. M., Villaluenga, I., Timachova, K. & Balsara, N. P. Diffusion and migration in polymer electrolytes. *Prog. Polym. Sci.* **103**, 101220 (2020).
10. Aziz, S. B., Woo, T. J., Kadir, M. F. Z. & Ahmed, H. M. A conceptual review on polymer electrolytes and ion transport models. *J. Sci. Adv. Mater. Devices* **3**, 1–17 (2018).
11. Zhou, L. et al. High areal capacity, long cycle life 4 V ceramic all-solid-state Li-ion batteries enabled by chloride solid electrolytes. *Nat. Energy* **7**, 83–93 (2022).
In this paper, a chlorospinel superionic conductor ($Li_2In_xSc_{0.666-x}Cl_4$) was used to demonstrate that chloride materials can have excellent stability against uncoated high-voltage cathode materials, with over 3,000 cycles at room temperature.
12. Kwak, H. et al. Emerging halide superionic conductors for all-solid-state batteries: design, synthesis, and practical applications. *ACS Energy Lett.* **7**, 1776–1805 (2022).
13. Nikodimos, Y., Su, W. & Hwang, B. J. Halide solid-state electrolytes: stability and application for high voltage all-solid-state Li batteries. *Adv. Energy Mater.* https://doi.org/10.1002/aenm.202202854 (2023).
14. Al-Salih, H., Houache, M. S. E., Baranova, E. A. & Abu-Lebdeh, Y. Composite cathodes for solid-state lithium batteries: 'catholytes' the underrated giants. *Adv. Energy Sustain. Res.* https://doi.org/10.1002/aesr.202200032 (2022).
15. Kim, M. et al. Carbon-free high-performance cathode for solid-state Li–O_2 battery. *Sci. Adv.* **8**, eabm8584 (2022).
16. Ma, S. B. et al. Mixed ionic–electronic conductor of perovskite $Li_xLa_yMO_{3-\delta}$ toward carbon-free cathode for reversible lithium–air batteries. *Adv. Energy Mater.* **10**, 2001767 (2020).
17. Nuernberg, R. B. Numerical comparison of usual Arrhenius-type equations for modelling ionic transport in solids. *Ionics* **26**, 2405–2412 (2020).
18. Qi, J. et al. Bridging the gap between simulated and experimental ionic conductivities in lithium superionic conductors. *Mater. Today Phys.* **21**, 100463 (2021).
19. Arbi, K., Tabellout, M., Lazarraga, M. G., Rojo, J. M. & Sanz, J. Non-Arrhenius conductivity in the fast lithium conductor $Li_{1.2}Ti_{1.8}Al_{0.2}(PO_4)_3$: a ^{7}Li NMR and electric impedance study. *Phys. Rev. B* **72**, 094302 (2005).
20. Winter, G. & Gómez-Bombarelli, R. Simulations with machine learning potentials identify the ion conduction mechanism mediating non-Arrhenius behavior in LGPS. *J. Phys. Energy* **5**, 024004 (2023).
21. Hargreaves, C. J. et al. A database of experimentally measured lithium solid electrolyte conductivities evaluated with machine learning. *npj Comput. Mater.* **9**, 9 (2023).
22. Fu, Z., Chen, X. & Zhang, Q. Review on the lithium transport mechanism in solid-state battery materials.*Wiley Interdiscip. Rev. Comput. Mol. Sci.* https://doi.org/10.1002/wcms.1621 (2022).
23. Gao, Y. et al. Classical and emerging characterization techniques for investigation of ion transport mechanisms in crystalline fast ionic conductors. *Chem. Rev.* **120**, 5954–6008 (2020).
24. Hodge, I. M., Ingram, M. D. & West, A. R. Impedance and modulus spectroscopy of polycrystalline solid electrolytes. *J. Electroanal. Chem. Interfacial Electrochem.* **74**, 125–143 (1976).
25. Lai, W. & Haile, S. M. Impedance spectroscopy as a tool for chemical and electrochemical analysis of mixed conductors: a case study of ceria. *J. Am. Ceram. Soc.* **88**, 2979–2997 (2005).
26. Kuhn, A., Duppel, V. & Lotsch, B. V. Tetragonal $Li_{10}GeP_2S_{12}$ and Li_7GePS_8 — exploring the Li ion dynamics in LGPS Li electrolytes. *Energy Environ. Sci.* **6**, 3548 (2013).
27. Kuhn, A. et al. NMR relaxometry as a versatile tool to study Li ion dynamics in potential battery materials. *Solid State Nucl. Magn. Reson.* **42**, 2–8 (2012).
28. Klenk, M. J. et al. Lithium self-diffusion in a model lithium garnet oxide $Li_5La_3Ta_2O_{12}$: a combined quasi-elastic neutron scattering and molecular dynamics study. *Solid State Ion.* **312**, 1–7 (2017).

29. Sugiyama, J. et al. Li-ion diffusion in $Li_4Ti_5O_{12}$ and $LiTi_2O_4$ battery materials detected by muon spin spectroscopy. *Phys. Rev. B* **92**, 014417 (2015).
30. Poletayev, A. D. et al. The persistence of memory in ionic conduction probed by nonlinear optics. *Nature* **625**, 691–696 (2024).
31. Poletayev, A. D., Dawson, J. A., Islam, M. S. & Lindenberg, A. M. Defect-driven anomalous transport in fast-ion conducting solid electrolytes. *Nat. Mater.* **21**, 1066–1073 (2022).
32. Frenkel, D. & Smit, B. in *Understanding Molecular Simulation* 2nd edn (eds Frenkel, D. & Smit, B.) 63–107 (Academic, 2002).
33. Henkelman, G. & Jónsson, H. Improved tangent estimate in the nudged elastic band method for finding minimum energy paths and saddle points. *J. Chem. Phys.* **113**, 9978–9985 (2000).
34. Henkelman, G., Jóhannesson, G. & Jónsson, H. in *Theoretical Methods in Condensed Phase Chemistry* (ed. Schwartz, S. D.) 269–302 (Kluwer Academic, 2002).
35. Brown, I. D. Recent developments in the methods and applications of the bond valence model. *Chem. Rev.* **109**, 6858–6919 (2009).
36. Adams, S. & Rao, R. P. Transport pathways for mobile ions in disordered solids from the analysis of energy-scaled bond-valence mismatch landscapes. *Phys. Chem. Chem. Phys.* **11**, 3210–3216 (2009).
37. Chen, D. et al. High throughput identification of Li ion diffusion pathways in typical solid state electrolytes and electrode materials by BV-Ewald method. *J. Mater. Chem. A* **7**, 1300–1306 (2018).
38. Onsager, L. Reciprocal relations in irreversible processes. I. *Phys. Rev.* **37**, 405–426 (1930).
39. Onsager, L. Reciprocal relations in irreversible processes. II. *Phys. Rev.* **38**, 2265–2279 (1931).
40. Prigogine, I. *Introduction to Thermodynamics of Irreversible Processes* 3rd edn (Wiley-Interscience, 1967).
41. Murch, G. E. The haven ratio in fast ionic conductors. *Solid State Ion.* **7**, 177–198 (1982).
42. Fong, K. D., Self, J., McCloskey, B. D. & Persson, K. A. Ion correlations and their impact on transport in polymer-based electrolytes. *Macromolecules* **54**, 2575–2591 (2021).
43. Wills, I. in *Thomas Edison: Success and Innovation through Failure* 203–222 (Springer, 2020).
44. Kasper, H. M. Series of rare earth garnets $Ln^{3+}{}_3M_2Li^+{}_3O_{12}$ (M = Te, W). *Inorg. Chem.* **8**, 1000–1002 (1969).
45. Thangadurai, V., Kaack, H. & Weppner, W. J. F. Novel fast lithium ion conduction in garnet-type $Li_5La_3M_2O_{12}$ (M = Nb, Ta). *J. Am. Ceram. Soc.* **86**, 437–440 (2003).
46. Li, Y., Han, J.-T., Wang, C.-A., Xie, H. & Goodenough, J. B. Optimizing Li^+ conductivity in a garnet framework. *J. Mater. Chem.* **22**, 15357–15361 (2012).
47. Aono, H., Sugimoto, E., Sadaoka, Y., Imanaka, N. & Adachi, G. Ionic conductivity and sinterability of lithium titanium phosphate system. *Solid State Ion.* **40**, 38–42 (1990).
48. Murugan, R., Thangadurai, V. & Weppner, W. Fast lithium ion conduction in garnet-type $Li_7La_3Zr_2O_{12}$. *Angew. Chem. Int Ed.* **46**, 7778–7781 (2007).
This paper reported that garnet-type oxides can be superionic conductors; they are one of the most widely studied solid electrolyte materials today.
49. Shon, Y.-J. & Min, K. Extracting chemical information from scientific literature using text mining: building an ionic conductivity database for solid-state electrolytes. *ACS Omega* https://doi.org/10.1021/acsomega.3c01424 (2023).
50. Wang, Y. et al. Design principles for solid-state lithium superionic conductors. *Nat. Mater.* **14**, 1026–1031 (2015).
In this paper, the authors established how different anion frameworks affect Li-ion conductivities, rationalizing the high ionic conductivities in many of the body-centred-cubic sulfide conductors.
51. Jun, K. et al. Lithium superionic conductors with corner-sharing frameworks. *Nat. Mater.* **21**, 924–931 (2022).
This paper rationalized that distorted Li-ion coordination environments as well as weak interaction between Li and non-Li cations lead to fast Li-ion diffusion in corner-sharing frameworks and presented 10 new oxide-based superionic conductors that share a similar structural feature.
52. Kamaya, N. et al. A lithium superionic conductor. *Nat. Mater.* **10**, 682–686 (2011).
53. Ong, S. P. et al. Phase stability, electrochemical stability and ionic conductivity of the $Li_{10\pm1}MP_2X_{12}$ (M = Ge, Si, Sn, Al or P, and X = O, S or Se) family of superionic conductors. *Energy Environ. Sci.* **6**, 148–156 (2012).
54. YAMANE, H. et al. Crystal structure of a superionic conductor, $Li_7P_3S_{11}$. *Solid State Ion.* **178**, 1163–1167 (2007).
55. Seino, Y., Ota, T., Takada, K., Hayashi, A. & Tatsumisago, M. A sulphide lithium super ion conductor is superior to liquid ion conductors for use in rechargeable batteries. *Energy Environ. Sci.* **7**, 627–631 (2014).
56. Kaup, K., Zhou, L., Huq, A. & Nazar, L. F. Impact of the Li substructure on the diffusion pathways in alpha and beta Li_3PS_4: an in situ high temperature neutron diffraction study. *J. Mater. Chem. A* **8**, 12446–12456 (2020).
57. Kimura, T. et al. Stabilizing high-temperature α-Li_3PS_4 by rapidly heating the glass. *J. Am. Chem. Soc.* **145**, 14466–14474 (2023).
58. Kaup, K. et al. Correlation of structure and fast ion conductivity in the solid solution series $Li_{1+2x}Zn_{1-x}PS_4$. *Chem. Mater.* **30**, 592–596 (2018).
59. Brant, J. A. et al. Fast lithium ion conduction in Li_2SnS_3: synthesis, physicochemical characterization, and electronic structure. *Chem. Mater.* **27**, 189–196 (2015).
60. Lin, Z., Liu, Z., Dudney, N. J. & Liang, C. Lithium superionic sulfide cathode for all-solid lithium–sulfur batteries. *ACS Nano* **7**, 2829–2833 (2013).
61. Roh, J., Lyoo, J. & Hong, S.-T. Enhanced Li-ion conductivity and air stability of Sb-substituted Li_4GeS_4 toward all-solid-state Li-ion batteries. *ACS Appl. Energy Mater.* **6**, 5446–5455 (2023).
62. Lyoo, J., Kim, H. J., Hyoung, J., Chae, M. S. & Hong, S.-T. Zn substituted $Li_4P_2S_6$ as a solid lithium-ion electrolyte for all-solid-state lithium batteries. *J. Solid State Chem.* **320**, 123861 (2023).
63. Liu, Z. et al. Anomalous high ionic conductivity of nanoporous β-Li_3PS_4. *J. Am. Chem. Soc.* **135**, 975–978 (2013).
64. Roh, J., Do, N., Manjón-Sanz, A. & Hong, S.-T. Li_2GeS_3: lithium ionic conductor with an unprecedented structural type. *Inorg. Chem.* **62**, 15856–15863 (2023).
65. Gamon, J. et al. Computationally guided discovery of the sulfide Li_3AlS_3 in the Li–Al–S phase field: structure and lithium conductivity. *Chem. Mater.* **31**, 9699–9714 (2019).
66. Murayama, M., Sonoyama, N., Yamada, A. & Kanno, R. Material design of new lithium ionic conductor, thio-LISICON, in the Li_2S–P_2S_5 system. *Solid State Ion.* **170**, 173–180 (2004).
67. Kimura, T. et al. Preparation and characterization of lithium ion conductive Li_3SbS_4 glass and glass-ceramic electrolytes. *Solid State Ion.* **333**, 45–49 (2019).
68. Kanno, R., Hata, T., Kawamoto, Y. & Irie, M. Synthesis of a new lithium ionic conductor, thio-LISICON–lithium germanium sulfide system. *Solid State Ion.* **130**, 97–104 (2000).
69. Kwak, H. et al. Li^+ conduction in air-stable Sb-substituted Li_4SnS_4 for all-solid-state Li-Ion batteries. *J. Power Sources* **446**, 227338 (2020).
70. Lim, H., Kim, S.-C., Kim, J., Kim, Y.-I. & Kim, S.-J. Structure of Li_5AlS_4 and comparison with other lithium-containing metal sulfides. *J. Solid State Chem.* **257**, 19–25 (2018).
71. Huber, S., Preitschaft, C., Weihrich, R. & Pfitzner, A. Preparation, crystal structure, electronic structure, impedance spectroscopy, and Raman spectroscopy of Li_3SbS_3 and Li_3AsS_3. *Z. Anorg. Allg. Chem.* **638**, 2542–2548 (2012).
72. Zhou, L., Minafra, N., Zeier, W. G. & Nazar, L. F. Innovative approaches to Li-argyrodite solid electrolytes for all-solid-state lithium batteries. *Acc. Chem. Res.* **54**, 2717–2728 (2021).
73. Richards, W. D., Wang, Y., Miara, L. J., Kim, J. C. & Ceder, G. Design of $Li_{1+2x}Zn_{1-x}PS_4$, a new lithium ion conductor. *Energy Environ. Sci.* **9**, 3272–3278 (2016).
74. Suzuki, N. et al. Synthesis and electrochemical properties of I^-4 type $Li_{1+2x}Zn_{1-x}PS_4$ solid electrolyte. *Chem. Mater.* https://doi.org/10.1021/acs.chemmater.7b03833 (2018).
75. Wang, C., Liang, J., Kim, J. T. & Sun, X. Prospects of halide-based all-solid-state batteries: from material design to practical application. *Sci. Adv.* **8**, eadc9516 (2022).
76. Wang, S. et al. Lithium chlorides and bromides as promising solid-state chemistries for fast ion conductors with good electrochemical stability. *Angew. Chem. Int. Ed.* **58**, 8039–8043 (2019).
77. Park, D. et al. Theoretical design of lithium chloride superionic conductors for all-solid-state high-voltage lithium-ion batteries. *ACS Appl. Mater. Interfaces* **12**, 34806–34814 (2020).
78. Kanno, R. & Murayama, M. Lithium ionic conductor thio-LISICON: the Li_2S GeS_2 P_2S_5 system. *J. Electrochem. Soc.* **148**, A742–A746 (2001).
79. Hong, H. Y.-P. Crystal structure and ionic conductivity of $Li_{14}Zn(GeO_4)_4$ and other new Li^+ superionic conductors. *Mater. Res Bull.* **13**, 117–124 (1978).
80. Aono, H. Ionic conductivity of solid electrolytes based on lithium titanium phosphate. *J. Electrochem. Soc.* **137**, 1023 (1990).
81. Kim, J., Kim, J., Avdeev, M., Yun, H. & Kim, S.-J. $LiTa_2PO_8$: a fast lithium-ion conductor with new framework structure. *J. Mater. Chem. A* **6**, 22478–22482 (2018).
82. Wang, Q. et al. A new lithium-ion conductor $LiTaSiO_5$: theoretical prediction, materials synthesis, and ionic conductivity. *Adv. Funct. Mater.* **29**, 1904232 (2019).
83. Xiong, S. et al. Computation-guided design of $LiTaSiO_5$, a new lithium ionic conductor with sphene structure. *Adv. Energy Mater.* **9**, 1803821 (2019).
84. Kang, K., Meng, Y. S., Bréger, J., Grey, C. P. & Ceder, G. Electrodes with high power and high capacity for rechargeable lithium batteries. *Science* **311**, 977–980 (2006).
85. der Ven, A. V. & Ceder, G. Lithium diffusion mechanisms in layered intercalation compounds. *J. Power Sources* **97**, 529–531 (2001).
86. Yu, S. et al. Design of a trigonal halide superionic conductor by regulating cation order–disorder. *Science* **382**, 573–579 (2023).
This paper reported that in the Li_3MCl_6 trigonal chloride superionic conductor, two factors, in-plane Li percolation paths and stacking interlayer distances, govern Li-ion conductivity, and they are inversely correlated with each other.
87. Peng, J. et al. Fast lithium ion conductivity in layered (Li-Ag)CrS_2. *J. Am. Chem. Soc.* https://doi.org/10.1021/jacs.0c08448 (2020).
88. Delmas, C. et al. On the behavior of the Li_xNiO_2 system: an electrochemical and structural overview. *J. Power Sources* **68**, 120–125 (1997).
89. Samsonov, G. V. *The Oxide Handbook* (Springer, 1973).
90. Jacobs, P. W. M. & Vernon, M. L. Defect energies for magnesium oxide and lithium oxide. *J. Chem. Soc. Faraday Trans.* **86**, 1233–1238 (1990).
91. Stefano, D. D. et al. Superionic diffusion through frustrated energy landscape. *Chem* **5**, 2450–2460 (2019).
This paper reported that in the novel superionic conductor $LiTi_2(PS_4)_3$ the highly distorted Li-ion sites provide a smooth and frustrated energy landscape.
92. Waroquiers, D. et al. Statistical analysis of coordination environments in oxides. *Chem. Mater.* https://doi.org/10.1021/acs.chemmater.7b02766 (2017).
93. Inaguma, Y., Katsumata, T., Itoh, M. & Morii, Y. Crystal structure of a lithium ion-conducting perovskite $La_{2/3-x}Li_{3x}TiO_3$ (x=0.05). *J. Solid State Chem.* **166**, 67–72 (2002).
94. Inaguma, Y. et al. High ionic conductivity in lithium lanthanum titanate. *Solid State Commun.* **86**, 689–693 (1993).
95. He, X. et al. Crystal structural framework of lithium super-ionic conductors. *Adv. Energy Mater.* **9**, 1902078 (2019).
96. Aono, H., Sugimoto, E., Sadaoka, Y., Imanaka, N. & Adachi, G. Ionic conductivity of the lithium titanium phosphate ($Li_{1+x}M_xTi_{2-x}(PO_4)_3$, M = Al, Sc, Y, and La) systems. *J. Electrochem. Soc.* **136**, 590–591 (1989).

97. Arbi, K., Mandal, S., Rojo, J. M. & Sanz, J. Dependence of ionic conductivity on composition of fast ionic conductors $Li_{1+x}Ti_{2-x}Al_x(PO_4)_3$, $0 \le x \le 0.7$. A parallel NMR and electric impedance study. *Chem. Mater.* **14**, 1091–1097 (2002).
98. Rossbach, A., Tietz, F. & Grieshammer, S. Structural and transport properties of lithium-conducting NASICON materials. *J. Power Sources* **391**, 1–9 (2018).
99. Cussen, E. J. Structure and ionic conductivity in lithium garnets. *J. Mater. Chem.* **20**, 5167–5173 (2010).
100. Xiao, Y. et al. Lithium oxide superionic conductors inspired by garnet and NASICON structures. *Adv. Energy Mater.* **11**, 2101437 (2021).
This paper suggested the concept of the activated diffusion network as the common feature of Li stuffing in garnet and NASICON-type superionic conductors, resulting in a graph-based criterion to search for materials similar to garnets and NASICONs.
101. Deng, B. et al. CHGNet as a pretrained universal neural network potential for charge-informed atomistic modelling. *Nat. Mach. Intell.* **5**, 1031–1041 (2023).
102. Kozinsky, B. et al. Effects of sublattice symmetry and frustration on ionic transport in garnet solid electrolytes. *Phys. Rev. Lett.* **116**, 055901 (2016).
103. Xu, M. et al. Mechanisms of Li^+ transport in garnet-type cubic $Li_{3+x}La_3M_2O_{12}$ (M = Te, Nb, Zr). *Phys. Rev. B* **85**, 052301 (2012).
104. Chen, Y. et al. Unlocking Li superionic conductivity in face-centred cubic oxides via face-sharing configurations. *Nat. Mater.* **23**, 535–542 (2024).
A face-centred-cubic anion sublattice is generally not considered favourable for Li-ion diffusion, but this paper showed that by introducing face-sharing Li configurations, superionic conductivity can be achieved in close-packed oxides.
105. Liu, H. et al. A disordered rock salt anode for fast-charging lithium-ion batteries. *Nature* **585**, 63–67 (2020).
106. Zhang, W. et al. Kinetic pathways of ionic transport in fast-charging lithium titanate. *Science* **367**, 1030–1034 (2020).
107. He, X., Zhu, Y. & Mo, Y. Origin of fast ion diffusion in super-ionic conductors. *Nat. Commun.* **8**, 15893 (2017).
This paper demonstrated that in many prototypical Li superionic conductors, Li-ion hops are correlated with each other, with multiple Li ions hopping simultaneously.
108. Liu, Y., Wang, S., Nolan, A. M., Ling, C., & Mo, Y. Tailoring the cation lattice for chloride lithium-ion conductors. *Adv. Energy Mater.* https://doi.org/10.1002/aenm.202002356 (2020).
109. Zhou, L. et al. A new halospinel superionic conductor for high-voltage all solid state lithium batteries. *Energy Environ. Sci.* **13**, 2056–2063 (2020).
110. Park, K.-H. et al. High-voltage superionic halide solid electrolytes for all-solid-state Li-ion batteries. *ACS Energy Lett.* **5**, 533–539 (2020).
111. Kvist, A. & Bengztelius, A. in *Fast Ion Transport in Solids* (ed. van Gool, W.) 193–199 (North-Holland, 1972).
112. Aronsson, R., Knape, H. E. G., Lundén, A., Nilsson, L. & Torell, L. M. Neutron, X-ray and Brillouin scattering studies of rotator phases with fast ion conduction. *Solid State Ion.* **5**, 445–447 (1981).
113. Dissanayake, M. A. K. L., Careem, M. A., Bandaranayake, P. W. S. K. & Wijayasekera, C. N. Ionic conductivity of solid solutions of α-Li_2SO_4 with Li_2WO_4: strong evidence for the paddle wheel mechanism of ion transport. *Solid State Ion.* **48**, 277–281 (1991).
114. Lundén, A. Enhancement of cation mobility in some sulphate phases due to a paddle-wheel mechanism. *Solid State Ion.* **28**, 163–167 (1988).
115. Secco, E. A. Electrical conductivity measurements to test for rotating sulfate ions in fast ion conductors. *Phys. Status Solidi* **88**, K75–K77 (1985).
116. Gundusharma, U. M., MacLean, C. & Secco, E. A. Rotating sulfate ion contribution to electrical conductivity in Li_2SO_4 and $LiNaSO_4$? *Solid State Commun.* **57**, 479–481 (1986).
117. Jansen, M. Volume effect or paddle-wheel mechanism — fast alkali-metal ionic conduction in solids with rotationally disordered complex anions. *Angew. Chem. Int. Ed. Engl.* **30**, 1547–1558 (1991).
118. Tsai, P. et al. Double paddle-wheel enhanced sodium ion conduction in an antiperovskite solid electrolyte. *Adv. Energy Mater.* **13**, 2203284 (2023).
119. Smith, J. G. & Siegel, D. J. Low-temperature paddlewheel effect in glassy solid electrolytes. *Nat. Commun.* **11**, 1483 (2020).
120. Zhang, Z., Roy, P.-N., Li, H., Avdeev, M. & Nazar, L. F. Coupled cation–anion dynamics enhances cation mobility in room-temperature superionic solid-state electrolytes. *J. Am. Chem. Soc.* **141**, 19360–19372 (2019).
121. Zhang, Z., & Nazar, L. F. Exploiting the paddle-wheel mechanism for the design of fast ion conductors. *Nat. Rev. Mater.* https://doi.org/10.1038/s41578-021-00401-0 (2022).
122. Zhang, Z. et al. Targeting superionic conductivity by turning on anion rotation at room temperature in fast ion conductors. *Matter* **2**, 1667–1684 (2020).
123. Verdal, N. et al. Anion reorientations in the superionic conducting phase of $Na_2B_{12}H_{12}$. *J. Phys. Chem. C* **118**, 17483–17489 (2014).
124. Dimitrievska, M. et al. Carbon incorporation and anion dynamics as synergistic drivers for ultrafast diffusion in superionic $LiCB_{11}H_{12}$ and $NaCB_{11}H_{12}$. *Adv. Energy Mater.* **8**, 1703422 (2018).
125. Sun, Y. et al. Rotational cluster anion enabling superionic conductivity in sodium-rich antiperovskite Na_3OBH_4. *J. Am. Chem. Soc.* **141**, 5640–5644 (2019).
126. Fang, H. & Jena, P. Argyrodite-type advanced lithium conductors and transport mechanisms beyond paddle-wheel effect. *Nat. Commun.* **13**, 2078 (2022).
127. Jun, K., Lee, B., Kam, R. & Ceder, G. The non-existence of a paddlewheel effect in superionic conductors. *Proc. Natl Acad. Sci. USA* **121**, e2316493121 (2024).
This paper investigated what types of rotational motion of anion groups exist in fast Li-ion conductors and showed that large-angle rotational motion as implied by the term 'paddlewheel effect' is not correlated to Li-ion diffusion.
128. Udovic, T. J. et al. Exceptional superionic conductivity in disordered sodium decahydro-*closo*-decaborate. *Adv. Mater.* **26**, 7622–7626 (2014).
129. Wilmer, D., Feldmann, H., Lechner, R. E. & Combet, J. Sodium ion conduction in plastic phases: dynamic coupling of cations and anions in the picosecond range. *J. Mater. Res.* **20**, 1973–1978 (2005).
130. Kweon, K. E. et al. Structural, chemical, and dynamical frustration: origins of superionic conductivity in *closo*-borate solid electrolytes. *Chem. Mater.* **29**, 9142–9153 (2017).
131. Hanghofer, I., Gadermaier, B. & Wilkening, H. M. R. Fast rotational dynamics in argyrodite-type Li_6PS_5X (X: Cl, Br, I) as seen by ^{31}P nuclear magnetic relaxation — on cation–anion coupled transport in thiophosphates. *Chem. Mater.* **31**, 4591–4597 (2019).
132. Brinek, M., Hiebl, C., Hogrefe, K., Hanghofer, I. & Wilkening, H. M. R. Structural disorder in Li_6PS_5I speeds ^7Li nuclear spin recovery and slows down ^{31}P relaxation — implications for translational and rotational jumps as seen by nuclear magnetic resonance. *J. Phys. Chem. C* **124**, 22934–22940 (2020).
133. Huynh, D. Q. Metrics for 3D rotations: comparison and analysis. *J. Math. Imaging Vis.* **35**, 155–164 (2009).
134. Rettie, A. J. E. et al. A two-dimensional type I superionic conductor. *Nat. Mater.* **20**, 1683–1688 (2021).
135. Gupta, M. K. et al. Fast Na diffusion and anharmonic phonon dynamics in superionic Na_3PS_4. *Energy Environ. Sci.* **14**, 6554–6563 (2021).
136. Gupta, M. K. et al. Strongly anharmonic phonons and their role in superionic diffusion and ultralow thermal conductivity of Cu_7PSe_6. *Adv. Energy Mater.* https://doi.org/10.1002/aenm.202200596 (2022).
137. Xu, Z., Chen, X., Zhu, H. & Li, X. Anharmonic cation–anion coupling dynamics assisted lithium-ion diffusion in sulfide solid electrolytes. *Adv. Mater.* **34**, 2207411 (2022).
138. Wang, H. et al. Borohydride substitution effects of Li_6PS_5Cl solid electrolyte. *ACS Appl. Energy Mater.* **4**, 12079–12083 (2021).
139. Sun, Y. et al. Enhanced ionic conductivity and lack of paddle-wheel effect in pseudohalogen-substituted Li argyrodites. *Matter* **5**, 4379–4395 (2022).
140. Han, J.-H. et al. Borohydride and halide dual-substituted lithium argyrodites. *Mater. Horiz.* **11**, 251–261 (2023).
141. Fang, H. & Jena, P. Li-rich antiperovskite superionic conductors based on cluster ions. *Proc. Natl Acad. Sci. USA* **114**, 11046–11051 (2017).
142. Jang, Y. et al. Lithium superionic conduction in BH_4-substituted thiophosphate solid electrolytes. *Adv. Sci.* **10**, 2204942 (2023).
143. Muy, S. et al. High-throughput screening of solid-state Li-ion conductors using lattice-dynamics descriptors. *iScience* **16**, 270–282 (2019).
144. Muy, S. et al. Tuning mobility and stability of lithium ion conductors based on lattice dynamics. *Energy Environ. Sci.* **11**, 850–859 (2018).
145. Muy, S., Schlem, R., Shao-Horn, Y. & Zeier, W. G. Phonon–ion interactions: designing ion mobility based on lattice dynamics. *Adv. Energy Mater.* https://doi.org/10.1002/aenm.202002787 (2020).
146. Deng, Y. et al. Enhancing the lithium ion conductivity in lithium superionic conductor (LISICON) solid electrolytes through a mixed polyanion effect. *ACS Appl. Mater. Inter.* **9**, 7050–7058 (2017).
147. Kraft, M. A. et al. Influence of lattice polarizability on the ionic conductivity in the lithium superionic argyrodites Li_6PS_5X (X = Cl, Br, I). *J. Am. Chem. Soc.* **139**, 10909–10918 (2017).
This paper systematically investigated the effect of anion framework polarizability on the ionic conductivity by tuning the fractional occupancy of halide ions in argyrodite-type superionic conductors, highlighting the importance of lattice stiffness on optimizing ionic conductivity.
148. Manthiram, A. & Goodenough, J. B. Lithium insertion into $Fe_2(SO_4)_3$ frameworks. *J. Power Sources* **26**, 403–408 (1989).
149. Etourneau, J., Portier, J. & Ménil, F. The role of the inductive effect in solid state chemistry: how the chemist can use it to modify both the structural and the physical properties of the materials. *J. Alloy. Compd.* **188**, 1–7 (1992).
150. Krauskopf, T., Culver, S. P. & Zeier, W. G. Bottleneck of diffusion and inductive effects in $Li_{10}Ge_{1-x}Sn_xP_2S$. *Chem. Mater.* **30**, 1791–1798 (2018).
151. Culver, S. P. et al. Evidence for a solid-electrolyte inductive effect in the superionic conductor $Li_{10}Ge_{1-x}Sn_xP_2S_{12}$. *J. Am. Chem. Soc.* https://doi.org/10.1021/jacs.0c10735 (2020).
This paper demonstrated that the change of chemical bonding within the framework of the $Li_{10}Ge_{1-x}Sn_xP_2S_{12}$ system and its effect on ionic conductivity (inductive) can be quantified, making it a viable strategy to optimize ionic conductivities.
152. Pareek, T. et al. $LiSnZr(PO_4)_3$: NASICON-type solid electrolyte with excellent room temperature Li^+ conductivity. *J. Alloy Compd.* **777**, 602–611 (2019).
153. Zhang, Z. et al. $Na_{11}Sn_2PS_{12}$: a new solid state sodium superionic conductor. *Energy Environ. Sci.* **11**, 87–93 (2017).
154. Yu, Z. et al. Exceptionally high ionic conductivity in $Na_3P_{0.62}As_{0.38}S_4$ with improved moisture stability for solid-state sodium-ion batteries. *Adv. Mater.* https://doi.org/10.1002/adma.201605561 (2017).
155. Zeng, Y. et al. High-entropy mechanism to boost ionic conductivity. *Science* **378**, 1320–1324 (2022).
This paper demonstrated that the high-entropy mechanism can improve ionic conductivities and elucidated how high entropy affects the site energy distributions to enhance lithium-ion conductivity.
156. Lin, J. et al. A high-entropy multicationic substituted lithium argyrodite superionic solid electrolyte. *ACS Mater. Lett.* **4**, 2187–2194 (2022).

157. Stramare, S., Thangadurai, V. & Weppner, W. Lithium lanthanum titanates: a review. *Chem. Mater.* **15**, 3974–3990 (2003).
158. Harada, Y., Ishigaki, T., Kawai, H. & Kuwano, J. Lithium ion conductivity of polycrystalline perovskite $La_{0.67-x}Li_{3x}TiO_3$ with ordered and disordered arrangements of the A-site ions. *Solid State Ion.* **108**, 407–413 (1998).
159. Harada, Y., Hirakoso, Y., Kawai, H. & Kuwano, J. Order–disorder of the A-site ions and lithium ion conductivity in the perovskite solid solution $La_{0.67-x}Li_{3x}TiO_3$ (x=0.11). *Solid State Ion.* **121**, 245–251 (1999).
This paper was presented at the 11th International Conference on Solid State Ionics, Hawaii, 1997.
160. Schlem, R. et al. Mechanochemical synthesis: a tool to tune cation site disorder and ionic transport properties of Li_3MCl_6 (M = Y, Er) superionic conductors. *Adv. Energy Mater.* **10**, 1903719 (2020).
This paper reported the use of various synthesis methods to tune the degree of cation disorder in $Li_3Y/ErCl_6$ and demonstrated that cation disorder obtained via mechanochemical synthesis results in substantially higher ionic conductivity.
161. Wang, K. et al. A cost-effective and humidity-tolerant chloride solid electrolyte for lithium batteries. *Nat. Commun.* **12**, 4410 (2021).
162. Liang, J., Li, X., Adair, K. R. & Sun, X. Metal halide superionic conductors for all-solid-state batteries. *Acc. Chem. Res.* **54**, 1023–1033 (2021).
163. Tanaka, Y. et al. New oxyhalide solid electrolytes with high lithium ionic conductivity >10 mS cm^{-1} for all-solid-state batteries. *Angew. Chem. Int. Ed.* **62**, e202217581 (2023).
This paper reported $LiMOCl_4$ (M = Ta, Nb), with an ionic conductivity of up to 12.4 mS cm^{-1} at room temperature, the highest among any non-sulfide-based conductors, opening up opportunities in the oxychloride chemistry.
164. Rayavarapu, P. R., Sharma, N., Peterson, V. K. & Adams, S. Variation in structure and Li^+-ion migration in argyrodite-type Li_6PS_5X (X = Cl, Br, I) solid electrolytes. *J. Solid State Electrochem.* **16**, 1807–1813 (2012).
165. Gautam, A. et al. Engineering the site-disorder and lithium distribution in the lithium superionic argyrodite Li_6PS_5Br. *Adv. Energy Mater.* https://doi.org/10.1002/aenm.202003369 (2020).
166. Morgan, B. J. Mechanistic origin of superionic lithium diffusion in anion-disordered Li_6PS_5X argyrodites. *Chem. Mater.* **33**, 2004–2018 (2021).
167. Liu, Z. et al. High ionic conductivity achieved in $Li_3Y(Br_3Cl_3)$ mixed halide solid electrolyte via promoted diffusion pathways and enhanced grain boundary. *ACS Energy Lett.* **6**, 298–304 (2021).
168. Kato, Y. et al. High-power all-solid-state batteries using sulfide superionic conductors. *Nat. Energy* **1**, 16030 (2016).
169. Feng, X., Chien, P.-H., Patel, S., Wang, Y. & Hu, Y.-Y. Enhanced ion conduction in $Li_{2.5}Zn_{0.25}PS_4$ via anion doping. *Chem. Mater.* **32**, 3036–3042 (2020).
170. Samson, A. J., Hofstetter, K., Bag, S. & Thangadurai, V. A bird's-eye view of Li-stuffed garnet-type $Li_7La_3Zr_2O_{12}$ ceramic electrolytes for advanced all-solid-state Li batteries. *Energy Environ. Sci.* **12**, 2957–2975 (2019).
171. Yu, C., Zhao, F., Luo, J., Zhang, L. & Sun, X. Recent development of lithium argyrodite solid-state electrolytes for solid-state batteries: synthesis, structure, stability and dynamics. *Nano Energy* **83**, 105858 (2021).
172. Hou, M., Liang, F., Chen, K., Dai, Y. & Xue, D. Challenges and perspectives of NASICON-type solid electrolytes for all-solid-state lithium batteries. *Nanotechnology* **31**, 132003 (2020).
173. Kato, Y., Hori, S., & Kanno, R. $Li_{10}GeP_2S_{12}$-type superionic conductors: synthesis, structure, and ionic transportation. *Adv. Energy Mater.* https://doi.org/10.1002/aenm.202002153 (2020).
174. Zheng, J., Perry, B. & Wu, Y. Antiperovskite superionic conductors: a critical review. *ACS Mater. Au* **1**, 92–106 (2021).
175. Li, X. et al. Progress and perspectives on halide lithium conductors for all-solid-state lithium batteries. *Energy Environ. Sci.* **13**, 1429–1461 (2020).
176. Bruce, P. G. & West, A. R. Ionic conductivity of LISICON solid solutions, $Li_{2+2x}Zn_{1-x}GeO_4$. *J. Solid State Chem.* **44**, 354–365 (1982).
177. Bruce, P. G. & West, A. R. Phase diagram of the LISICON, solid electrolyte system, Li_4GeO_4–Zn_2GeO_4. *Mater. Res. Bull.* **15**, 379–385 (1980).
178. Whiteley, J. M., Woo, J. H., Hu, E., Nam, K.-W. & Lee, S.-H. Empowering the lithium metal battery through a silicon-based superionic conductor. *J. Electrochem. Soc.* **161**, A1812–A1817 (2014).
179. Bron, P. et al. $Li_{10}SnP_2S_{12}$: an affordable lithium superionic conductor. *J. Am. Chem. Soc.* **135**, 15694–15697 (2013).
180. Bron, P., Dehnen, S. & Roling, B. $Li_{10}Si_{0.3}Sn_{0.7}P_2S_{12}$ — a low-cost and low-grain-boundary-resistance lithium superionic conductor. *J. Power Sources* **329**, 530–535 (2016).
181. Yang, K., Dong, J., Zhang, L., Li, Y. & Wang, L. Dual doping: an effective method to enhance the electrochemical properties of $Li_{10}GeP_2S_{12}$-based solid electrolytes. *J. Am. Ceram. Soc.* **98**, 3831–3835 (2015).
182. Sun, Y., Suzuki, K., Hori, S., Hirayama, M. & Kanno, R. Superionic conductors: $Li_{10+\delta}[Sn_ySi_{1-y}]_{1+\delta}P_{2-\delta}S_{12}$ with a $Li_{10}GeP_2S_{12}$-type structure in the Li_3PS_4–Li_4SnS_4–Li_4SiS_4 quasi-ternary system. *Chem. Mater.* **29**, 5858–5864 (2017).
183. Li, Y. et al. A lithium superionic conductor for millimeter-thick battery electrode. *Science* **381**, 50–53 (2023).
This paper showed that using a high-entropy mechanism, an LGPS-type superionic conductor can reach a conductivity of up to 32 mS cm^{-1} at room temperature.
184. Goodenough, J. B., Hong, H. Y.-P. & Kafalas, J. A. Fast Na^+-ion transport in skeleton structures. *Mater. Res. Bull.* **11**, 203–220 (1976).
185. Taylor, B. E., English, A. D. & Berzins, T. New solid ionic conductors. *Mater. Res. Bull.* **12**, 171–181 (1977).
186. Yamamoto, H., Tabuchi, M., Takeuchi, T., Kageyama, H. & Nakamura, O. Ionic conductivity enhancement in $LiGe_2(PO_4)_3$ solid electrolyte. *J. Power Sources* **68**, 397–401 (1997).
187. Arbi, K., Rojo, J. M. & Sanz, J. Lithium mobility in titanium based Nasicon $Li_{1+x}Ti_{2-x}Al_x(PO_4)_3$ and $LiTi_{2-x}Zr_x(PO_4)_3$ materials followed by NMR and impedance spectroscopy. *J. Eur. Ceram. Soc.* **27**, 4215–4218 (2007).
188. Subramanian, M. A., Subramanian, R. & Clearfield, A. Lithium ion conductors in the system $AB(IV)_2(PO_4)_3$ (B = Ti, Zr and Hf). *Solid State Ion.* **18**, 562–569 (1986).
189. Yi, E. et al. Materials that can replace liquid electrolytes in Li batteries: superionic conductivities in $Li_{1.7}Al_{0.3}Ti_{1.7}Si_{0.4}P_{2.6}O_{12}$. Processing combustion synthesized nanopowders to free standing thin films. *J. Power Sources* **269**, 577–588 (2014).
190. Liu, M. et al. Facile synthesis and electrochemical properties of high lithium ionic conductivity $Li_{1.7}Al_{0.3}Ti_{1.7}Si_{0.4}P_{2.6}O_{12}$ ceramic solid electrolyte. *J. Alloys Compd.* **756**, 103–110 (2018).
191. Thangadurai, V., Narayanan, S. & Pinzaru, D. Garnet-type solid-state fast Li ion conductors for Li batteries: critical review. *Chem. Soc. Rev.* **43**, 4714–4727 (2014).
192. Geiger, C. A. et al. Crystal chemistry and stability of '$Li_7La_3Zr_2O_{12}$' garnet: a fast lithium-ion conductor. *Inorg. Chem.* **50**, 1089–1097 (2011).
193. Vema, S., Berge, A. H., Nagendran, S. & Grey, C. P. Clarifying the dopant local structure and effect on ionic conductivity in garnet solid-state electrolytes for lithium-ion batteries. *Chem. Mater.* **35**, 9632–9646 (2023).
194. O'Callaghan, M. P. & Cussen, E. J. Lithium dimer formation in the Li-conducting garnets $Li_{5+x}Ba_xLa_{3-x}Ta_2O_{12}$ ($0<x\leq1.6$). *Chem. Commun.* **2007**, 2048–2050 (2007).
195. Xie, H., Alonso, J. A., Li, Y., Fernández-Díaz, M. T. & Goodenough, J. B. Lithium distribution in aluminum-free cubic $Li_7La_3Zr_2O_{12}$. *Chem. Mater.* **23**, 3587–3589 (2011).
196. Jalem, R. et al. Concerted migration mechanism in the Li ion dynamics of garnet-type $Li_7La_3Zr_2O_{12}$. *Chem. Mater.* **25**, 425–430 (2013).
197. Awaka, J., Kijima, N., Hayakawa, H. & Akimoto, J. Synthesis and structure analysis of tetragonal $Li_7La_3Zr_2O_{12}$ with the garnet-related type structure. *J. Solid State Chem.* **182**, 2046–2052 (2009).
198. Wolfenstine, J., Rangasamy, E., Allen, J. L. & Sakamoto, J. High conductivity of dense tetragonal $Li_7La_3Zr_2O_{12}$. *J. Power Sources* **208**, 193–196 (2012).
199. Deiseroth, H.-J. et al. Li_6PS_5X: a class of crystalline li-rich solids with an unusually high Li^+ mobility. *Angew. Chem. Int. Ed.* **47**, 755–758 (2008).
200. Kam, R. L. et al. Crystal structures and phase stability of the Li_2S–P_2S_5 system from first principles. *Chem. Mater.* **35**, 9111–9126 (2023).
201. Deiseroth, H. et al. Li_7PS_6 and Li_6PS_5X (X: Cl, Br, I): possible three-dimensional diffusion pathways for lithium ions and temperature dependence of the ionic conductivity by impedance measurements. *Z. Anorg. Allg. Chem.* **637**, 1287–1294 (2011).
202. Ziolkowska, D. A., Arnold, W., Druffel, T., Sunkara, M. & Wang, H. Rapid and economic synthesis of a Li_7PS_6 solid electrolyte from a liquid approach. *ACS Appl. Mater. Interfaces* **11**, 6015–6021 (2019).
203. Patel, S. V. et al. Tunable lithium-ion transport in mixed-halide argyrodites $Li_{6-x}PS_{5-x}ClBr_x$: an unusual compositional space. *Chem. Mater.* **33**, 1435–1443 (2021).
204. Zhou, L., Assoud, A., Zhang, Q., Wu, X. & Nazar, L. F. New family of argyrodite thioantimonate lithium superionic conductors. *J. Am. Chem. Soc.* **141**, 19002–19013 (2019).
This paper demonstrated that Sb substitution and modification of Li content can lead to an ionic conductivity of 24 mS cm^{-1} at room temperature, one of the highest values reported for the argyrodite family.
205. Baktash, A., Reid, J. C., Roman, T. & Searles, D. J. Diffusion of lithium ions in lithium-argyrodite solid-state electrolytes. *npj Comput. Mater.* **6**, 162 (2020).
206. Feng, X. et al. Enhanced ion conduction by enforcing structural disorder in Li-deficient argyrodites $Li_{6-x}PS_{5-x}Cl_{1+x}$. *Energy Storage Mater.* **30**, 67–73 (2020).
207. Yu, C. et al. Enabling ultrafast ionic conductivity in Br-based lithium argyrodite electrolytes for solid-state batteries with different anodes. *Energy Storage Mater.* **30**, 238–249 (2020).
208. Jung, W. D. et al. Superionic halogen-rich li-argyrodites using in situ nanocrystal nucleation and rapid crystal growth. *Nano Lett.* **20**, 2303–2309 (2020).
209. Yu, C. et al. Superionic conductivity in lithium argyrodite solid-state electrolyte by controlled Cl-doping. *Nano Energy* **69**, 104396 (2020).
210. Zhang, Z. et al. Enhancing ionic conductivity of solid electrolyte by lithium substitution in halogenated Li-argyrodite. *J. Power Sources* **450**, 227601 (2020).
211. Schneider, H. et al. Stabilization of highly conductive lithium argyrodites by means of lithium substitution: the case of $Li_6Fe_{0.5}PS_6$. *ChemistrySelect* **4**, 3351–3354 (2019).
212. Zhang, Z. et al. Design and synthesis of room temperature stable Li-argyrodite superionic conductors via cation doping. *J. Mater. Chem. A* https://doi.org/10.1039/c8ta10790d (2019).
213. Minafra, N., Culver, S. P., Krauskopf, T., Senyshyn, A. & Zeier, W. G. Effect of Si substitution on the structural and transport properties of superionic Li-argyrodites. *J. Mater. Chem. A* **6**, 645–651 (2017).
214. Schneider, H. et al. A novel class of halogen-free, super-conductive lithium argyrodites: synthesis and characterization. *J. Power Sources* **366**, 151–160 (2017).
215. Kraft, M. A. et al. Inducing high ionic conductivity in the lithium superionic argyrodites $Li_{6+x}P_{1-x}Ge_xS_5I$ for all-solid-state batteries. *J. Am. Chem. Soc.* https://doi.org/10.1021/jacs.8b10282 (2018).
216. Kanno, R., Takeda, Y., Takada, K. & Yamamoto, O. Phase diagram and ionic conductivity of the lithium chloride–iron(II) chloride system. *Solid State Ion.* **9**, 153–156 (1983).

217. Steiner, H. -J. & Lutz, H. D. Neue schnelle Ionenleiter vom Typ MMIIICl6 (MI = Li, Na, Ag; MIII = In, Y). *Z. Anorg. Allg. Chem.* **613**, 26–30 (1992).
218. Asano, T. et al. Solid halide electrolytes with high lithium-ion conductivity for application in 4 V class bulk-type all-solid-state batteries. *Adv. Mater.* **30**, 1803075 (2018).
This paper demonstrated that Li_3YCl_6 and Li_3YBr_6 are superionic conductors at room temperature, which led to extensive research in close-packed chloride chemistries for Li-ion conductors.
219. Li, X. et al. Structural regulation of halide superionic conductors for all-solid-state lithium batteries. *Nat. Commun.* **15**, 53 (2024).
220. Wang, Q. et al. Designing lithium halide solid electrolytes. *Nat. Commun.* **15**, 1050 (2024).
221. Li, X. et al. Origin of superionic $Li_3Y_{1-x}In_xCl_6$ halide solid electrolytes with high humidity tolerance. *Nano Lett.* **20**, 4384–4392 (2020).
222. Chen, S. et al. Enabling ultrafast lithium-ion conductivity of Li_2ZrCl_6 by indium doping. *Chin. Chem. Lett.* **33**, 4635–4639 (2022).
223. Kwak, H. et al. New cost-effective halide solid electrolytes for all-solid-state batteries: mechanochemically prepared Fe^{3+}-substituted Li_2ZrCl_6. *Adv. Energy Mater.* **11**, 2003190 (2021).
224. Tomita, Y., Fuji-i, A., Ohki, H., Yamada, K. & Okuda, T. New lithium ion conductor Li_3InBr_6 studied by ^{7}Li NMR. *Chem. Lett.* **27**, 223–224 (1998).
225. Li, X. et al. Air-stable Li_3InCl_6 electrolyte with high voltage compatibility for all-solid-state batteries. *Energy Environ. Sci.* **2019**, 2665–2671 (2019).
226. Liang, J. et al. Site-occupation-tuned superionic Li_xScCl_{3+x} halide solid electrolytes for all-solid-state batteries. *J. Am. Chem. Soc.* **142**, 7012–7022 (2020).
227. Lutz, H. D., Schmidt, W. & Haeuseler, H. Chloride spinels: a new group of solid lithium electrolytes. *J. Phys. Chem. Solids* **42**, 287–289 (1981).
228. Luo, J. et al. Halide superionic conductors with non-close-packed anion frameworks. *Angew. Chem. Int. Ed.* **63**, e202400424 (2024).
229. Kim, R. et al. Computational design and experimental synthesis of air-stable solid-state ionic conductors with high conductivity. *Chem. Mater.* **33**, 6909–6917 (2021).
230. Adams, S. Origin of fast Li^+-ion conductivity in the compressible oxyhalide LiNbOCl4. *Energy Storage Mater.* **38**, 103359 (2024).
231. Jun, K., Wei, G. & Ceder, G. Thermodynamic stability and diffusion mechanism of LiMXCl4 superionic conductors. Preprint at https://doi.org/10.26434/chemrxiv-2024-nm8ks (2024).
232. Yin, Y.-C. et al. A $LaCl_3$-based lithium superionic conductor compatible with lithium metal. *Nature* **616**, 77–83 (2023).
This paper reported the development of a new type of non-close-packed $LaCl_3$ superionic conductor obtained by stuffing extra Li into the structure and introducing La vacancies, demonstrating that non-close-packed chlorides can exhibit superionic conductivity.
233. Malik, R., Burch, D., Bazant, M. & Ceder, G. Particle size dependence of the ionic diffusivity. *Nano Lett.* **10**, 4123–4127 (2010).
234. Zhong, P., Gupta, S., Deng, B., Jun, K. & Ceder, G. Effect of cation disorder on lithium transport in halide superionic conductors. *ACS Energy Lett.* **9**, 2775–2781 (2024).
235. Batatia, I. et al. A foundation model for atomistic materials chemistry. Preprint at https://arxiv.org/abs/2401.00096 (2023).
236. Min, J., Gubow, L. M., Hargrave, R. J., Siegel, J. B. & Li, Y. Direct measurements of size-independent lithium diffusion and reaction times in individual polycrystalline battery particles. *Energy Environ. Sci.* **16**, 3847–3859 (2023).
237. Kahle, L., Marcolongo, A. & Marzari, N. High-throughput computational screening for solid-state Li-ion conductors. *Energy Environ. Sci.* https://doi.org/10.1039/c9ee02457c (2020).
238. Zhang, Y. et al. Unsupervised discovery of solid-state lithium ion conductors. *Nat. Commun.* **10**, 5260 (2019).
239. Sebti, E. et al. Stacking faults assist lithium-ion conduction in a halide-based superionic conductor. *J. Am. Chem. Soc.* **144**, 5795–5811 (2022).
240. Gautam, A. et al. Rapid crystallization and kinetic freezing of site-disorder in the lithium superionic argyrodite Li_6PS_5Br. *Chem. Mater.* **31**, 10178–10185 (2019).
241. Szymanski, N. J. et al. An autonomous laboratory for the accelerated synthesis of novel materials. *Nature* **624**, 86–91 (2023).
242. Lunt, A. M. et al. Modular, multi-robot integration of laboratories: an autonomous workflow for solid-state chemistry. *Chem. Sci.* **15**, 2456–2463 (2023).
243. Chen, J. et al. Navigating phase diagram complexity to guide robotic inorganic materials synthesis. *Nat. Synth.* **3**, 606–614 (2023).
244. Chen, C., Lu, Z. & Ciucci, F. Data mining of molecular dynamics data reveals Li diffusion characteristics in garnet $Li_7La_3Zr_2O_{12}$. *Sci. Rep.* **7**, 40769 (2017).
245. Jain, A. et al. Commentary. The Materials Project: a materials genome approach to accelerating materials innovation. *APL Mater.* **1**, 011002 (2013).

Acknowledgements

This work was funded by the Assistant Secretary of Energy Efficiency and Renewable Energy, Vehicle Technologies Office of the US Department of Energy (DOE), under contract number DE-AC02-05CH11231 under the Advanced Battery Materials (BMR) programme. Earlier work was performed with the support of Samsung Electronics. Earlier computational work utilized the resources of the National Energy Research Scientific Computing Center (NERSC), a US Department of Energy Office of Science user facility, as well as the clusters at the National Renewable Energy Laboratory (NREL) under *saepssic* and *ahlssic* allocations. K.J. acknowledges support from Kwanjeong Educational Foundation scholarship. G.W. acknowledges support by the US DOE, Office of Science, Office of Advanced Scientific Computing Research, Department of Energy Computational Science Graduate Fellowship under award number DE-SC0023112. This report was prepared as an account of work sponsored by an agency of the United States Government. Neither the United States Government nor any agency thereof, nor any of their employees, makes any warranty, express or implied, or assumes any legal liability or responsibility for the accuracy, completeness or usefulness of any information, apparatus, product or process disclosed, or represents that its use would not infringe privately owned rights. Reference herein to any specific commercial product, process or service by trade name, trademark, manufacturer, or otherwise does not necessarily constitute or imply its endorsement, recommendation or favouring by the United States Government or any agency thereof. The views and opinions of authors expressed herein do not necessarily state or reflect those of the United States Government or any agency thereof.

Author contributions

K.J., Y.C., G.W. and X.Y. researched data for the article. K.J. and G.C. led the drafting of the manuscript. All authors contributed substantially to discussion of the content and drafting of the article. K.J. and G.C. reviewed and/or edited the manuscript before submission.

Competing interests

The authors declare no competing interests.

Additional information

Peer review information *Nature Reviews Materials* thanks James Dawson and Yoon Seok Jung for their contribution to the peer review of this work.